HYSTORE

Hybrid Services from Advanced Thermal Energy Storage Systems

D2.2 Report on the characterization of the pre-selected materials for HYSTORE solutions I-III

1. Table of Contents

2. List of Figures

3. List of Tables

PROJECT DURATION: 1 January 2023 – 31 December 2026

GRANT AGREEMENT ID: 1010967 (Innovation Action)

WP: 2 **DELIVERABLE:** 2.2

LEAD BENEFICIARY: KTH

SUBMISSION DATE: 17 September 2024

DISSEMINATION LEVEL: Public

DUE DATE: M12

HYSTORE Website: https://www.hystore-project.eu/

REVISION HISTORY:

DATE	VERSION	AUTHOR/CONTRIBUTOR	REVISION BY	COMMENTS
01-12-2023	0.0	KTH & RUBI	-	
16-12-2023	0.1	KTH & RUBI		
17/09/2024	2.1		ARC	

DISCLAIMER

ACKNOWLEDGEMENT

This project has received funding from the European Union's Horizon Europe research and innovation programme under grant agreement N° 1010967.

Funded by the European Union

"Funded by the European Union. Views and opinions expressed are however those of the author(s) only and do not necessarily reflect those of the European Union or European Climate, Infrastructure and Environment Executive Agency (CINEA). Neither the European Union nor the granting authority can be held responsible for them."

4. Executive Summary

HYSTORE project aims to deliver modular plug-and-play compact thermal energy storage (TES) solutions using latent heat TES (LHTES) with phase change materials (PCMs) and thermochemical TES (TCS) with thermochemical heat storage materials (TCMs). These will be used and optimized for capturing flexible sector coupling of thermal and electrical sectors through their contributions in the building energy systems. Four TES solutions are here considered for different climate conditions and demonstration sites. This report concerns the characterization of the PCMs (along T2.2) that were already pre-selected (within T2.1), to fulfil the operational conditions of the HYSTORE solutions I, II and III, namely:

I: PCM ALL-IN-ONE solution (developed by AIT)

II: PCM LOW-TEMP. HEATING & COOLING solution (developed by RUBI)

III: PCM HEATING solution (developed by KTH)

The pre-selection of PCMs in T2.1 yielded several alternatives per HYSTORE solution (detailed more in D2.1). These were further shortlisted based on the specific design conditions of solutions I-III and the respective room-temperature corrosion of the candidates against the specific LHTES heat exchanger (HEX) materials (aluminum, polymer and stainless steel). Thereby, up to two optimal PCMs were chosen for each solution and mode (heating or cooling), namely:

I: PCM ALL-IN-ONE solution --> RT57HC & RT60HC (heating) and RT8HC, SP12sk and SP31 (cooling)

II: PCM LOW-TEMP. HEATING & COOLING solution --> SP31 & SP45 (heating) and RT 8HC & SP12sk (cooling)

III: PCM HEATING solution --> RT 57HC and RT60HC (heating)

Their thermophysical properties (thermal, mechanical and chemical behavior) such as heat capacity, density, corrosion (long-term at high temperature) and long-term cycling performance (hysteresis, supercooling, storage capacity and power, so on) in bench-scale were then characterized within T2.2. The employed methods and the corresponding results are presented and their relevance and suitability for HYSTORE solutions are discussed. Upon initial screening, several PCM choices (e.g., RT 60HC, RT 57HC, RT 8HC and SP31, per this intermediate screening), that could optimally cater to the operational conditions of HYSTORE solutions I, II and III, were short-listed at this pre-selection stage. The final PCM choices from these intermediate short-listing will be considered in the upcoming analyses and discussed in D 2.1.

5. Introduction

This section presents concisely the report summary, the relation of the tasks detailed herein to the rest of the HYSTORE project activities, contributions of the partners to this deliverable D2.2. The section ends with an outline of the deliverable.

5.1. Summary

TES is an indispensable component to realize climate neutral energy systems, within the context that 50% of the final energy use goes to heating and cooling today globally [1]. Compact TES and therein PCM-TES are relevant to move beyond the state-of-the-art that mainly lies in sensible TES which has comparatively much lower specific storage capacity. Selecting robust PCMs that fulfil the specific TES design criteria and maintain them consistently through long-term cycling is critical for the long-term success of PCM-TES systems.

The objective of this deliverable (within T2.2) is to present the experimental characterization of these important properties (along the thermal, mechanical and chemical behavior) of several PCMs that were shortlisted through an extensive screening at an earlier step (in T2.1). Therein, this provides recommendations of optimal PCMs for implementation in HYSTORE solutions I-III in the upcoming project phases.

5.2. Relation to other activities

The shortlisted PCM candidates' extensive characterization regime presented here for T2.2 is a follow-up step of T2.1, which concerned PCMs initial screening, considering an extensive list with certain material-scale property characterizations. The results and conclusions of this report will be directly used in the first place in T2.1 and for D2.1 for the final selection and thereafter in the next tasks of WP2: T 2.4 – design of the storage HEX and T2.5- Modular design and selection of Auxiliary. The D2.2 results also directly affect the final TES system operation, therefore directly influencing the WP3- storage system and low-level controller development, manufacturing and lab testing, as a whole.

5.3. Contribution of Partners

KTH (Energy Technology- EGI) is the task responsible and editor of this D2.2 report. RUBI is a key partner and a contributor for this report, for being the official PCM partner who has done the material-level characterizations and have been part of the conceptualization of the bench-scale test procedure at KTH, for the latter together with AIT. This report therefore also has content that coincides with some of parts of D2.1 that will be delivered a few months after D2.2, concerning PCMs screening and final optimal PCM selection (which on the other hand also depends on D2.2 conclusions).

5.4. Structure of the Deliverable

This deliverable D2.2 report is structured as follows:

- Section 6 details the first-stage initial screening of PCMs, considering ***material-intrinsic property (including corrosion) testing***. This encompasses concise explanation of the employed materials and characterization methods **by RUBI** (calorimetric analysis, corrosion tests, and other), plus the density and the high-temperature corrosion analyses done **by KTH** and the discussion of the obtained results. Section ends with concise specific concluding remarks (with recommendations) on this initial screening step at material-level.
- Section 0 presents the ***high-density PCM physical property testing at bench-scale*** conducted **by KTH,** comprising concise materials and methods (of the bench-scale long-term cycling tests and data analysis) details and the discussion of the results obtained. Lastly, specific concluding remarks are brought forward concerning bench-scale level analysis.
- Section 8 presents conclusions from T2.2 in this D2.2 combining outcomes from both section 6 and 0, as relevant to the upcoming steps dependent on this deliverable, and also in general terms for the design of PCM-TES systems for similar applications.

6. First-stage initial screening of PCMs

This section presents the characterization of pre-selected PCMs for solutions I-III done by AIT, RUBI and KTH. Hereby the various thermophysical properties such as heat storage capacity, density and melting area are shown. The tests were done in a laboratory environment.

6.1. Materials and Methods – Intrinsic Property and Corrosion Characterization

The selection of PCMs is linked to different criteria, measuring methods and environmental impacts of the material. Some points and testing methods were already given in the proposal. Therefore, we are able to use organic (paraffins, fatty acids, alcohols, among others) and inorganic (salt hydrates, nitrate or nitrite salts).

6.1.1. PCM-selection criteria

The main properties sought after were:

- Operating range,
- Biobased,
- Long-term stability,
- Heat storage capacity,
- material compatibility (for HEX and containers etc.),
- availability and
- costs

In-addition, for each HYSTORE solution, their specific operational conditions were considered as summarized in Table 1 below:

Table 1. Specific operating conditions for each HYSTORE solution

Solution I: PCM ALL-IN-ONE (AIT)	**Solution II: LOW-TEMP. PCM HEATING & COOLING (RUBI)**	**Solution III: PCM HEATING (KTH)**
• Average storage temperature ~60 °C • Sharp peak during solidification for domestic hot water (DHW) • Heating with secondary loop stainless steel (SS) HEX to 50°C • Size of the thermal storage capacity about 186 l • Density ~800 kg/m³ • Non-corrosive against aluminum • organic PCM • Heat storage capacity >200 kJ/kg (55.6Wh/kg)	• Low temperature cooling: average storage temperature ~8 °C • Plan: research activity inorganic PCM 40-45°C • Updated conditions project site: PCM ~30°C for low temperature heating • Long-term stable through separation inhibitors • Non-corrosive against polymeric materials • Non-flammable	• 5-10 K temperature difference with heat transfer fluid (HTF) - Freezing ≥ 40-45 °C - Melting ≤ 55-60 °C • Average ~50 °C • Approximate PCM volume: 750 l • On HTF side approximately: - @PCM freezing: inlet ~25-35 °C (outdoor@10°C) - @PCM melting: inlet ~65 °C (outdoor@10°C)

6.1.2. Calorimetric method (standard evaluation)

The calorimetric method (as the standard evaluation) for measuring various thermophysical properties was done with a 3-layer-calorimeter. The "heat flow optimized temperature curve analysis" (WOTKA) in a 3-layer calorimeter (see Figure 1) is a method of measuring the heat storage capacity, melting- and crystallization temperature in sample sizes of 100 ml. As a cost-effective alternative to conventional measurement methods, PCMs based on paraffins and salt hydrates with several individual components can also be characterized for their heat storage capacity. The heating and cooling rate is 0.2 K/min in the temperature range from –20 to +100°C. For calibration we used water and hexadecane (99%).

Figure 1: three-layer calorimeter [2]

The sample (Figure 2) of approx. 100 ml (liquid material, powder or bulk material) to be tested is filled as vacuum tight as possible into a composite film (dimensions 220 x 150 mm) and shrink-wrapped. It is then folded in the middle and the temperature sensor is placed in between. The calorimeter is then closed with an insulated lid. The outside and inside temperatures are logged with a measuring rate of one value per minute.

Figure 2: sample size for WOTKA-measurement [2]

Figure 3: sample insertion in calorimetric measurement device [2]

Figure 4: closed WOTKA-device [2]

6.1.3. Initial-screened Materials

PCMs use phase transitions (solid-liquid, solid-solid, liquid-gas) in addition to the specific heat capacity of the storage material to store large amounts of energy with a high energy density. The phase change from solid to liquid and vice versa is considered here. The thermal energy is stored in a concealed manner, i.e., in contrast to sensitive heat storage systems such as water, the storage and retrieval of thermal energy leads to virtually no change in temperature. The geometry and materials of the PCM encapsulation play a decisive role in the efficiency and thermal output of the storage system (contact surface and contact time with the circulating medium).

Solution I: PCM ALL-IN-ONE

For solution I PCM ALL-IN-ONE (heating application), Rubitherm have selected some suitable PCMs in the temperature range 55-65°C based on already available data that passed the first screening considering all the constraints from the project. This also includes the need for reliable pilot installation. This selection is: RT57HC, RT60, RT60HC, RT62HC, RT64HC (all organic) and SP58 (inorganic). Note that for the cooling application, the selection of material candidates is reported in the following section together with materials for solution II.

For the specific operational conditions from 6.1.3, only RT57HC and RT60HC are matching the requirements. Both were extensively tested at RUBI and KTH. The already available partial enthalpies of these PCMs are shown in Figure and Figure. Their temperature and enthalpy curves are shown in Figure 6, Figure 7, Figure 8 and Figure 9 below. (Based on the analysis method described in section 6.1.2).

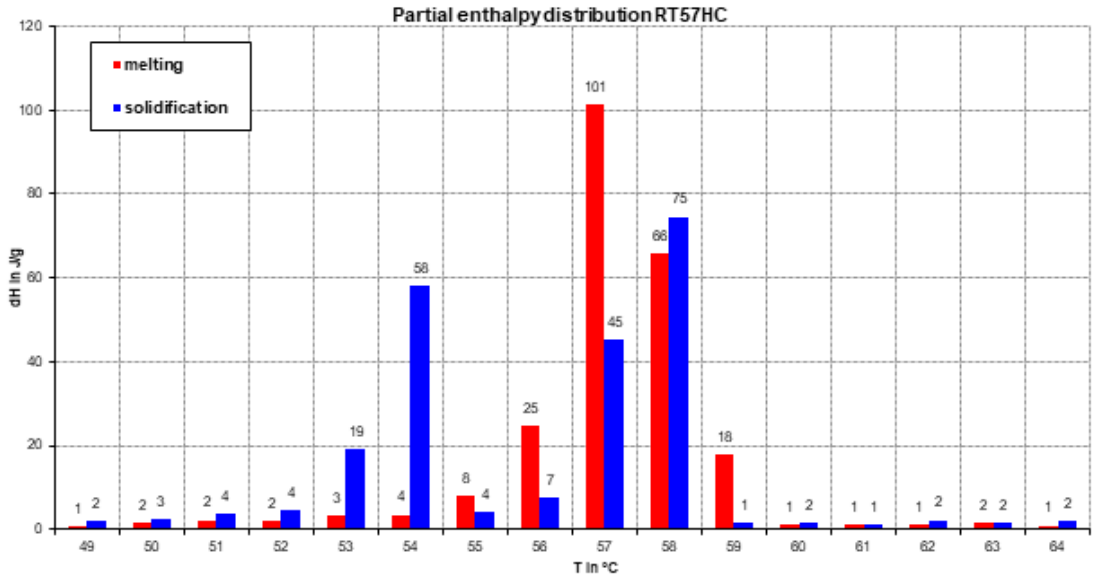

Figure 5. partial enthalpy of RT57HC in the temperature range 49-64°C

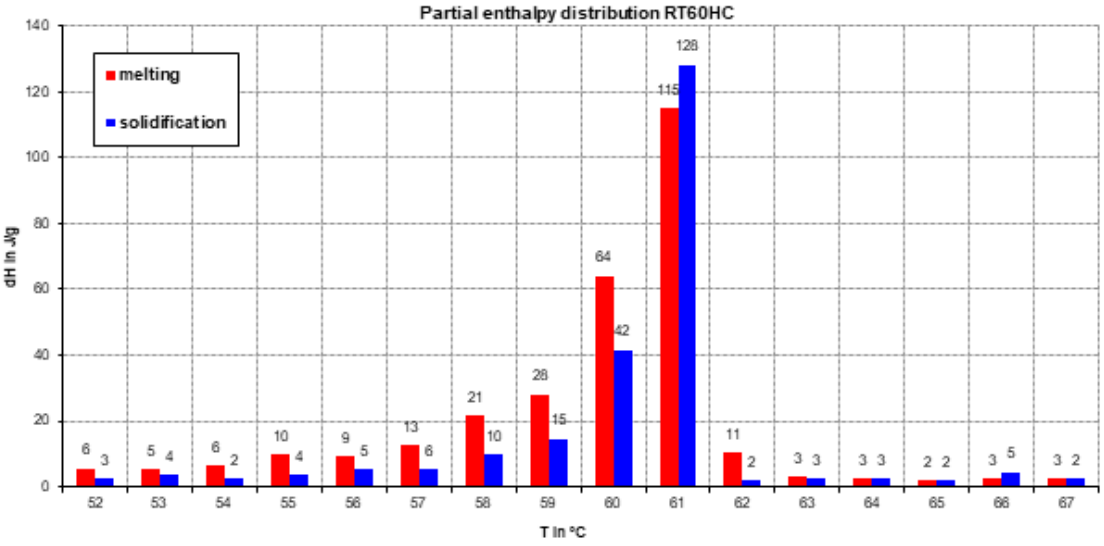

Figure6. partial enthalpy of RT60HC

In these diagrams above the partial enthalpy in J/g are shown on the y-axis and the temperature is presented on the x-axis. Melting and solidification enthalpies are presented in bars.

RT57HC shows two different peaks for freezing and one sharp peak for melting. The RT60HC has one sharp peak for melting and solidification.

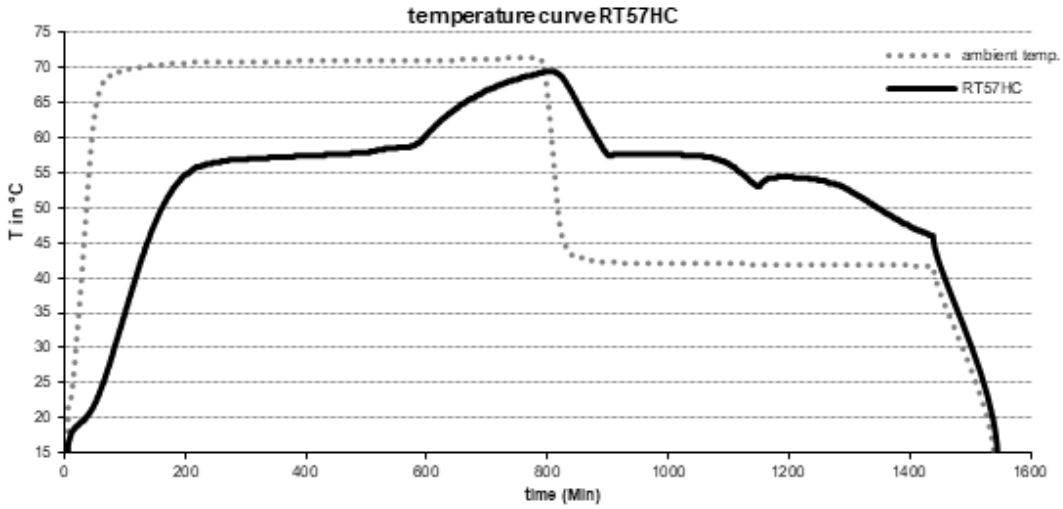

Figure 6. temperature curve of RT57HC

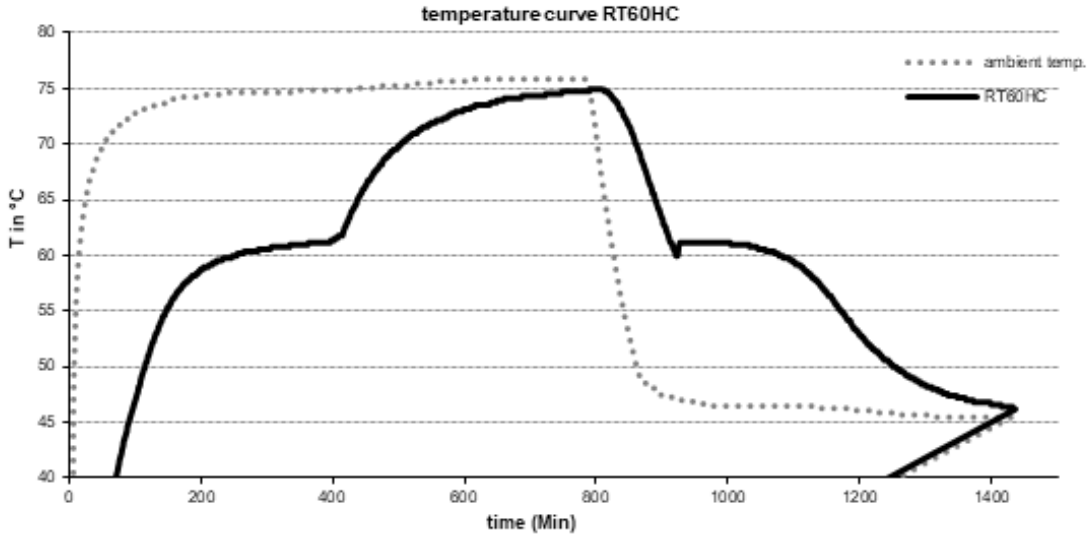

Figure 7: temperature curve of RT60HC

In these diagrams you can see the temperature curves of both materials. The first increase of temperature is called sensible range. The following plateau is the so called "latent heat area" and the second rise in temperature is again a sensible area. As already mentioned above there are two cooling plateaus for RT57HC in **Error! Reference source not found.**, while RT60HC h as only one cooling plateau.

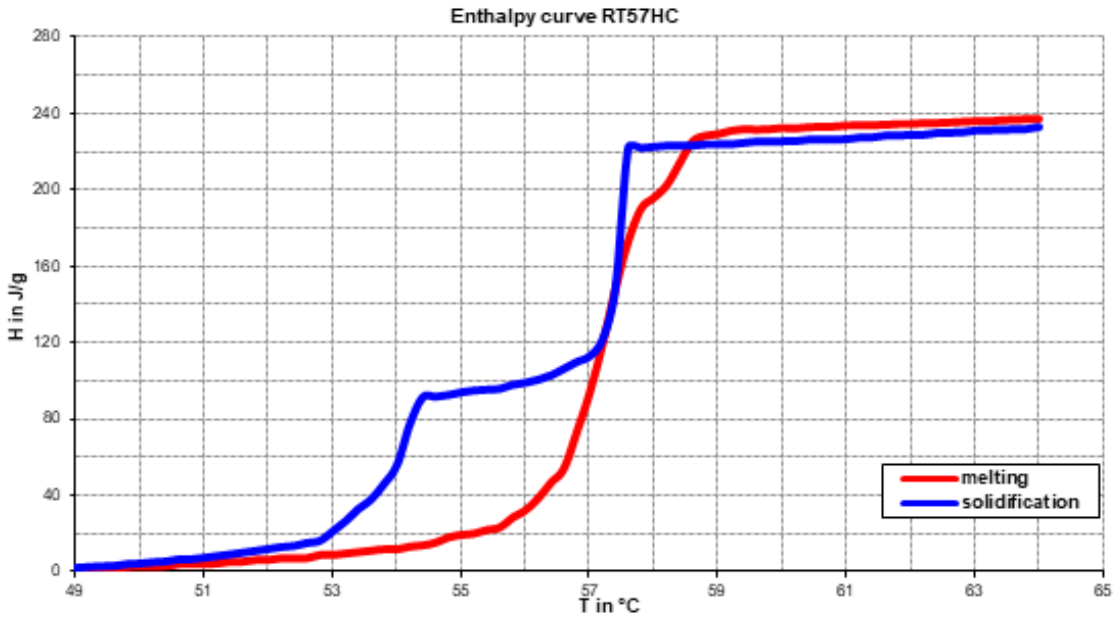

Figure 8: enthalpy curve of RT57HC

As can be seen in Figure 8 there is a second enthalpy plateau between 53.5°C and 57°C in the cooling curve.

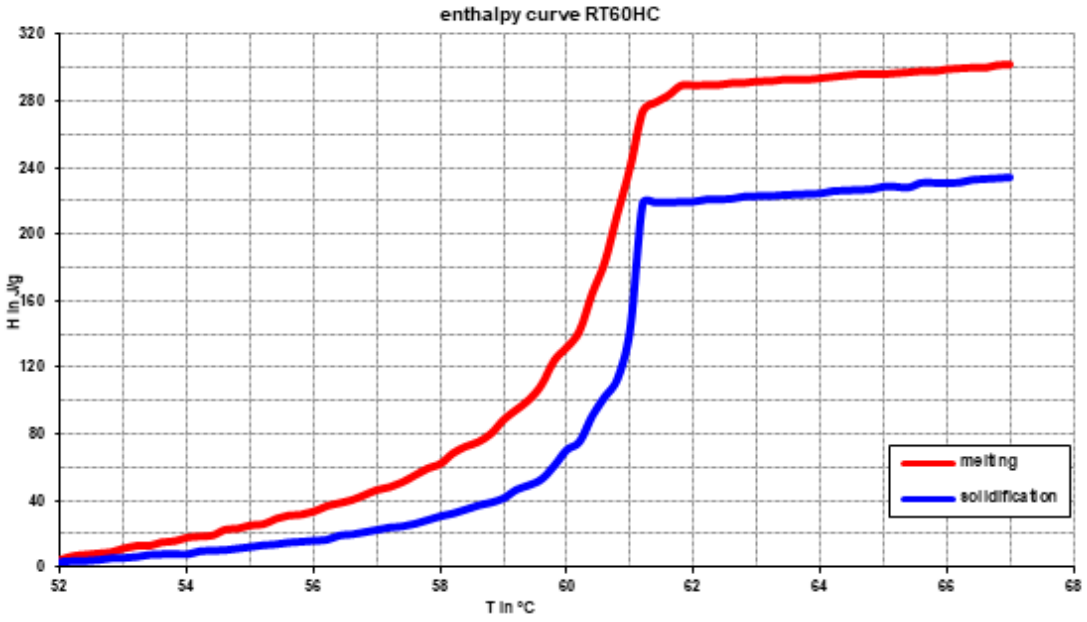

Figure 9: enthalpy curve of RT60HC

The enthalpy diagram of RT60HC, as in Figure 9 shows no such a second enthalpy plateau[1] and for this it is well suitable as a PCM for ALL-IN-ONE. The main thermophysical properties of both PCMs are listed in Table 2**Error! Reference source not found.**.

Table 2: main thermophysical properties of possible PCMs for temperature range 55-65°C

properties	RT57HC	RT60HC
Melting area [°C]	57-58	58-61
Freezing area [°C]	57-56	60-58
Heat storage capacity [kJ/kg] [Wh/kg]; T.-range	230/63; 50°C-65°C	210/58; 53°C-68°C
Specific heat capacity [kJ/kg*K]	2	2
Density solid [kg/l]	0.99	0.85
Density liquid [kg/l]	0.85	0.75
Max. Operation temperature [°C]	85	90
Biobased?	Yes	yes
Corrosion [-]	No Corrosive effect on metals	No corrosive effect on metals

Solution II: LOW-TEMP. HEATING&COOLING

For solution II LOW TEMP COOLING (and solution I cooling) there are three possible PCM candidates: RT8HC (organic), SP9 and SP12sk (both inorganic). The thermophysical properties are listed below in Table 3**Error! Reference source not found.**.

Table 3: main thermophysical properties of possible PCM for temperature range 8-10°C

properties	RT8HC	SP9	SP12sk
Melting area [°C]	7-9	10-11	12-13
Freezing area [°C]	8-7	9-7	11-10
Heat storage capacity [kJ/kg] [Wh/kg]; T.-range	190 / 53; 1°C-15°C	170 / 47; 2°C-16°C	160 / 44; 5°C-20°C
Specific heat capacity [kJ/kg*K]	2	2	2
Density solid [kg/l]	0.88	1.35	1.3
Density liquid [kg/l]	0.77	1.3	1.3

[1] Freezing often is faster and has a clear-cut phase change while melting is wider and so tends to spread the phase change. The differences here between melting and freezing shows this difference more, while per phase change enthalpy (i.e., enthalpy difference during phase change).

Max. Operation temperature [°C]	40	30	45
Biobased?	no	yes	yes
Corrosion [-]	No corrosive effect on metals	corrosive effect on metals	Corrosive effect on metals

An aluminum heat exchanger is used for tests with RT8HC (organic) and a polymer HEX is used for the tests with SP9 and SP12sk (inorganic). The analyzed thermophysical properties of RT8HC are summarized in Figure 10, Figure 11 and Figure 12. The SP9 and SP12sk were not tested yet, and is work in progress, because that these are experiments for the first characterization and what are the outcomes in terms of material characteristics.

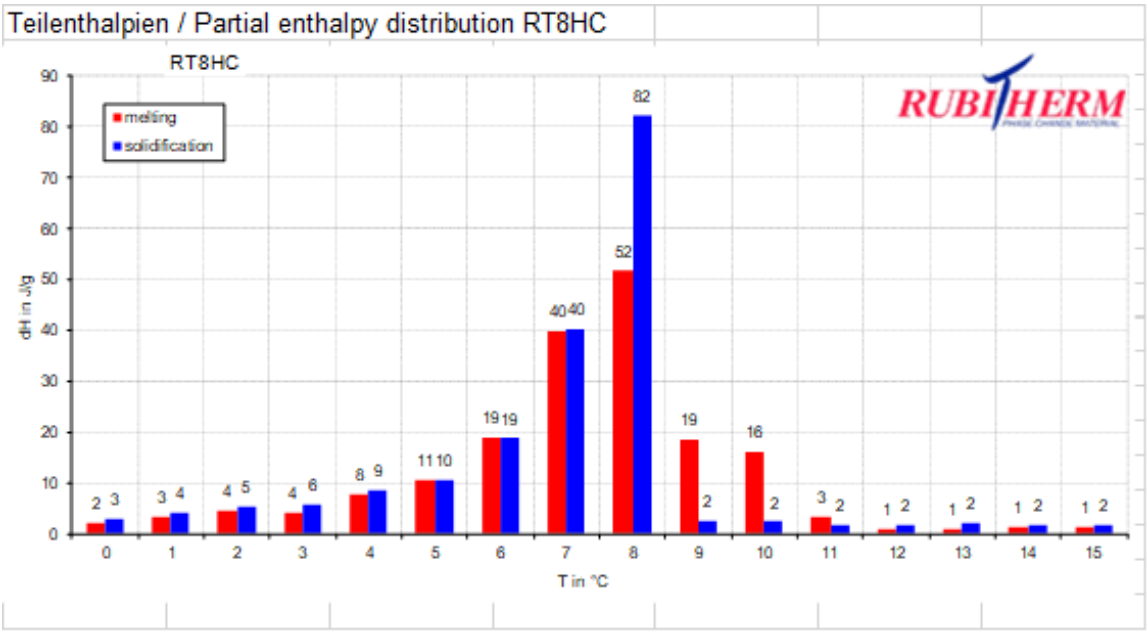

Figure 10: partial enthalpy of RT8HC

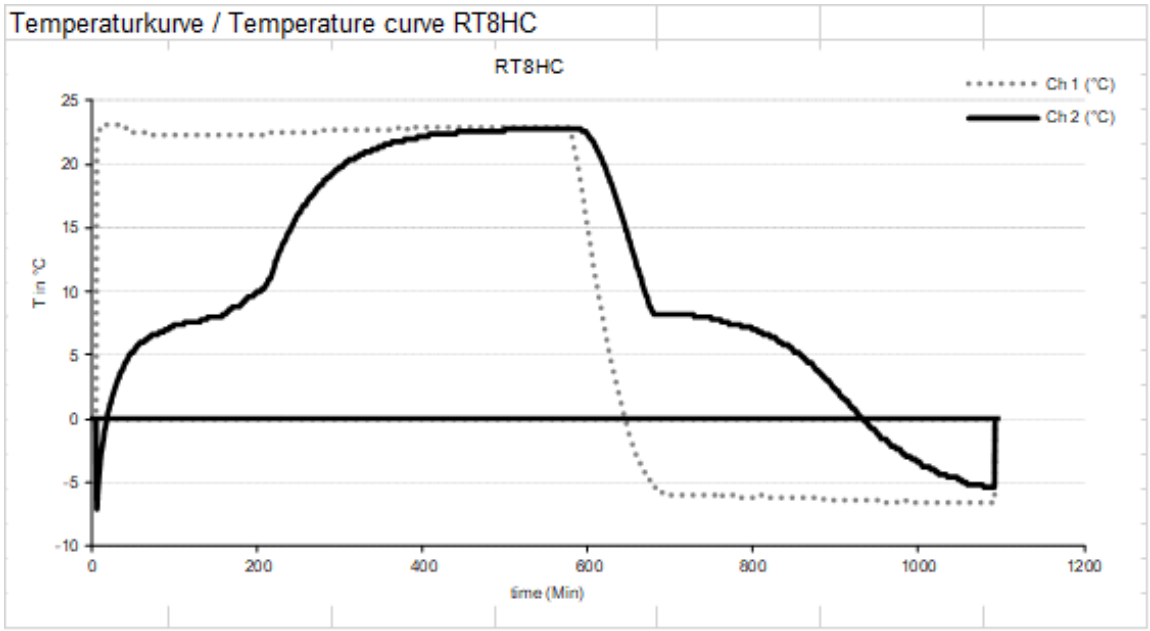

Figure 11: temperature curve of RT8HC

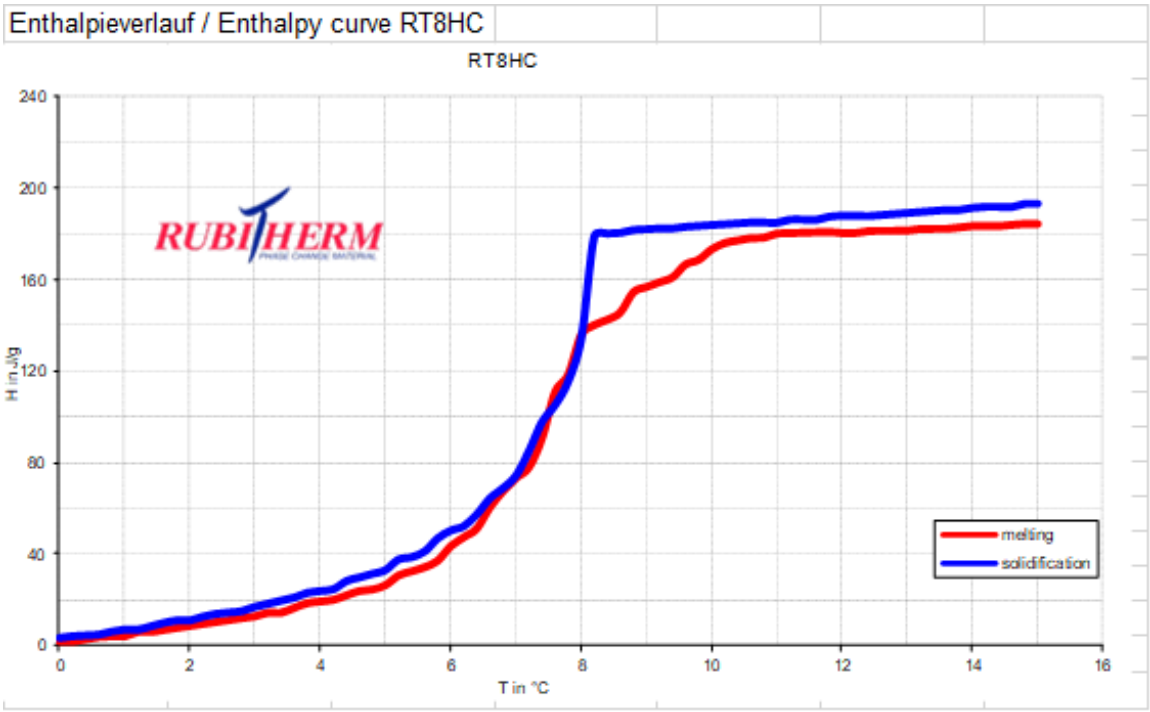

Figure 12: enthalpy curve of RT8HC

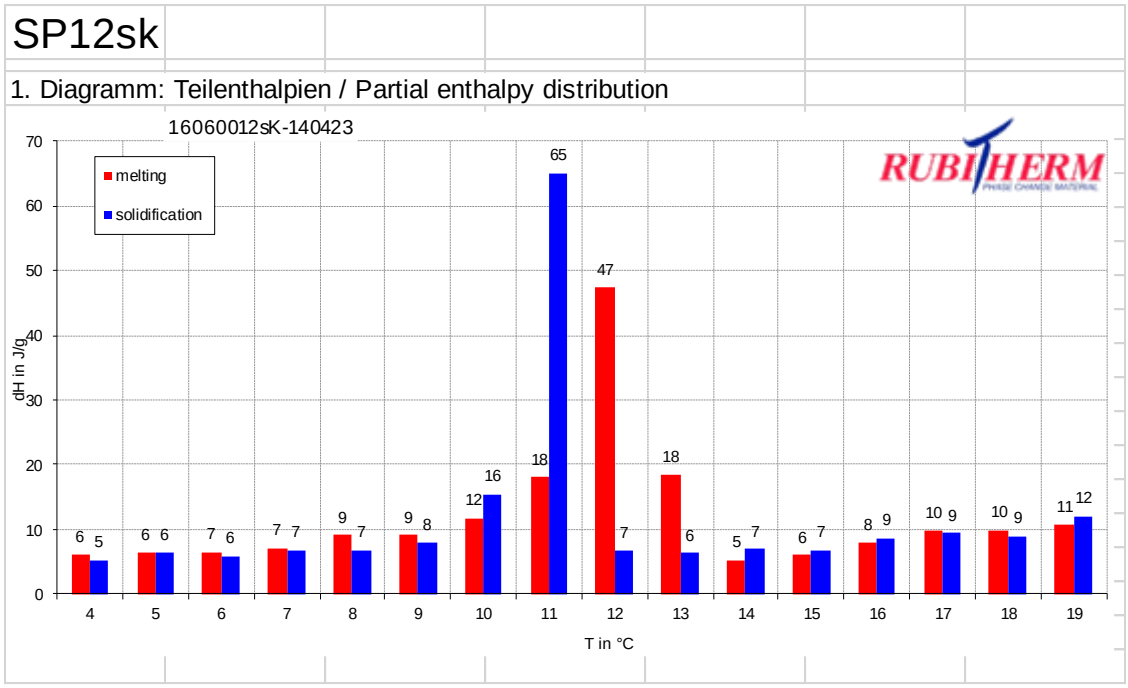

Figure 13: partial enthalpy of SP12sk

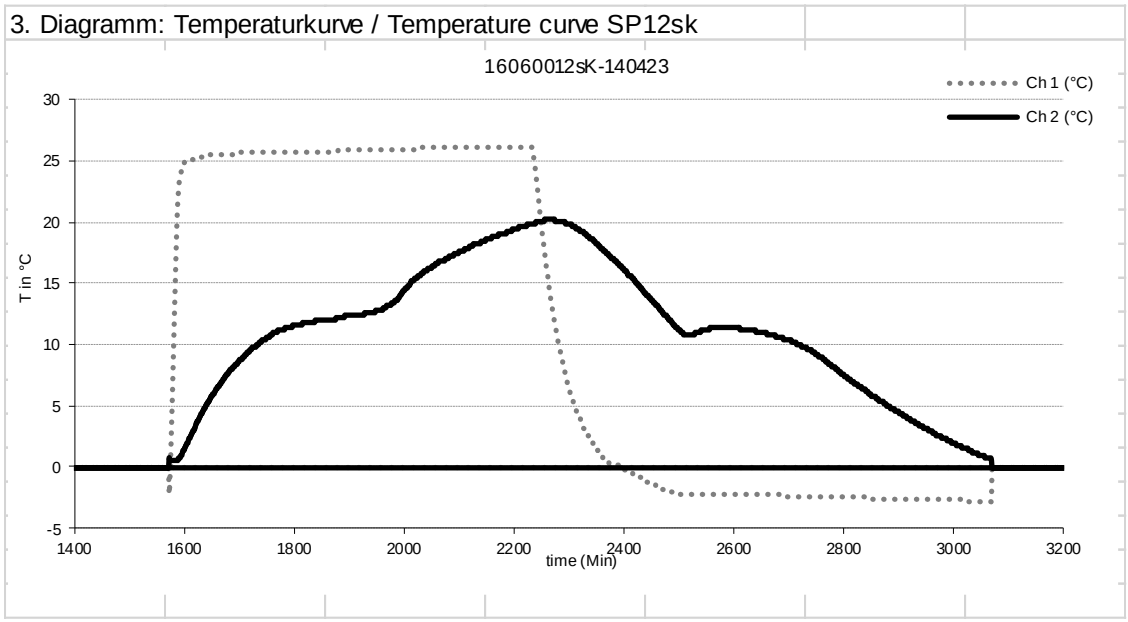

Figure 14: temperature curve of SP12sk

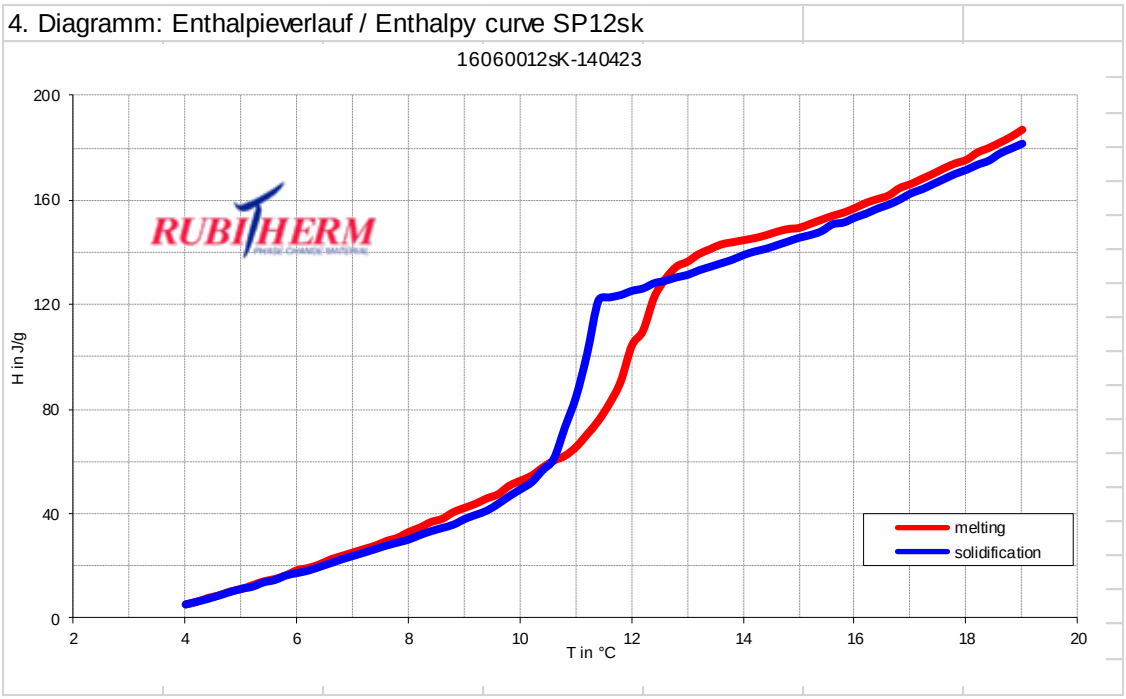

Figure 15: enthalpy curve of SP12sk

For further tests (with SP9 and SP12sk), a polymer HEX will be installed and filled with inorganic PCM.

For the LOW TEMP HEATING solution II further research and development was done. The aim was to find a good PCM for the temperature range 40°C-45°C. Several experimental PCMs were tested at Rubitherm. These tests include calorimetric measurements and long-term stability (testing of cycles). The partial enthalpy, temperature and enthalpy curves of SP41 are shown in Figure 16, Figure 17 and Figure 18, while the same property curves for SP45p2 after 265 cycles of testing are shown in Figure 19, Figure 20 and Figure 21. . SP41 shows a slightly wider temperature range than SP45p2 (sharp peaks for melting and solidification). There are 2 sharp peaks for melting and solidification, but the temperature range is no longer included. As you can see the subcooling of SP45p2 is lower to zero than SP41 which is a good propertie for an inorganic PCM.

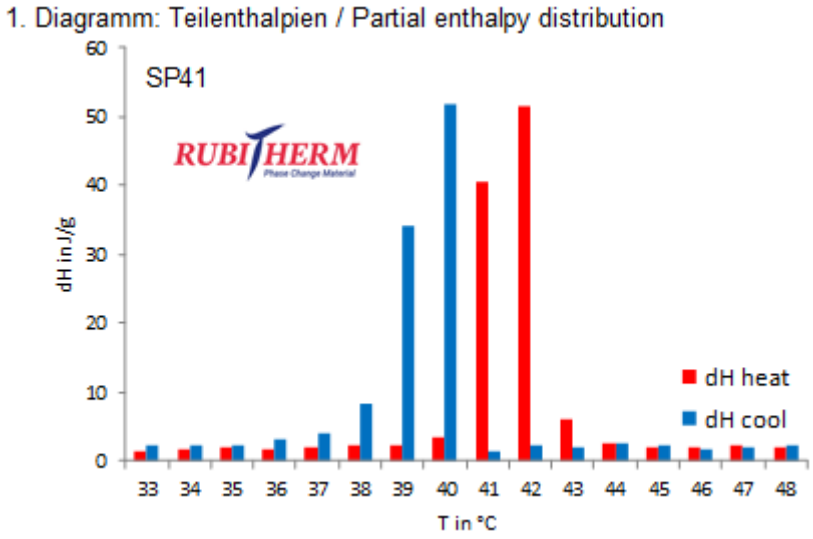

Figure 16: partial enthalpy of SP41

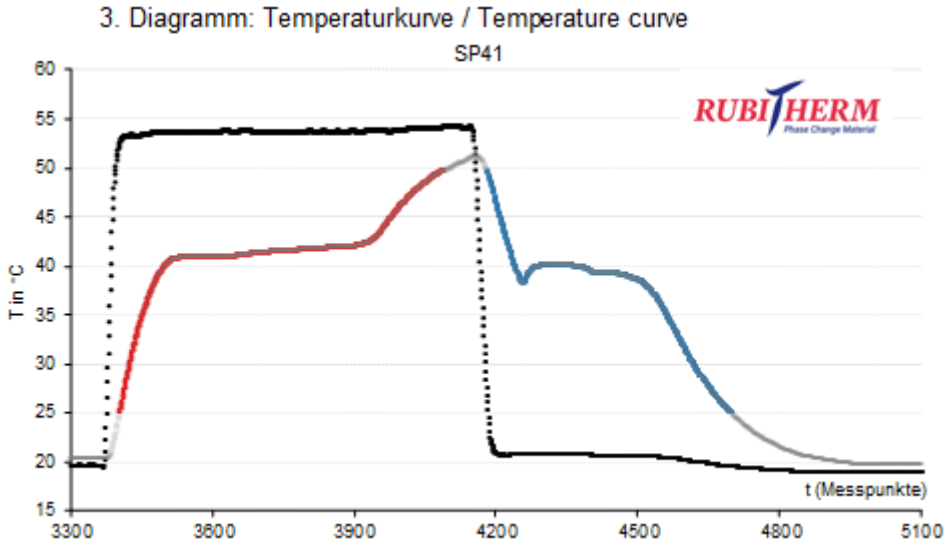

Figure 17: temperature curve of SP41

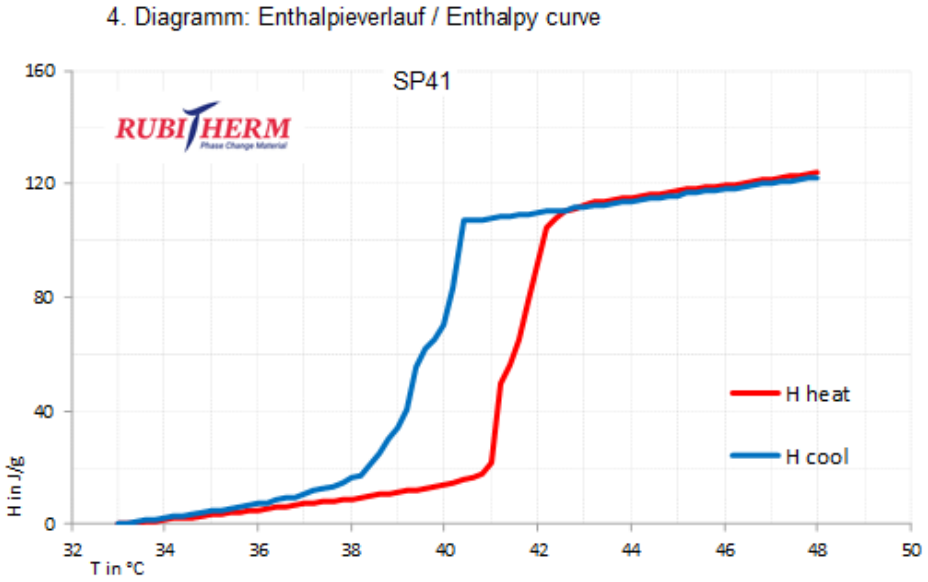

Figure 18: enthalpy curve of SP41

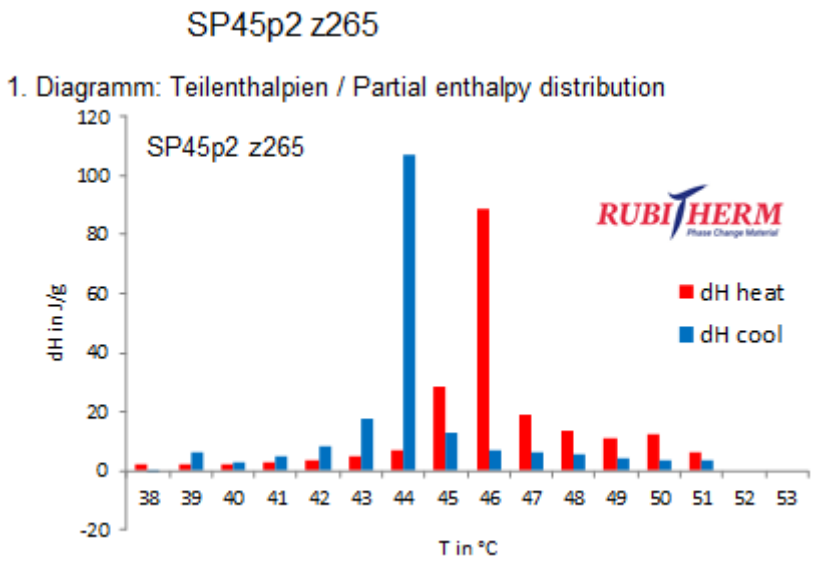

Figure 19: partial enthalpy of SP45p2 after 265 cycles

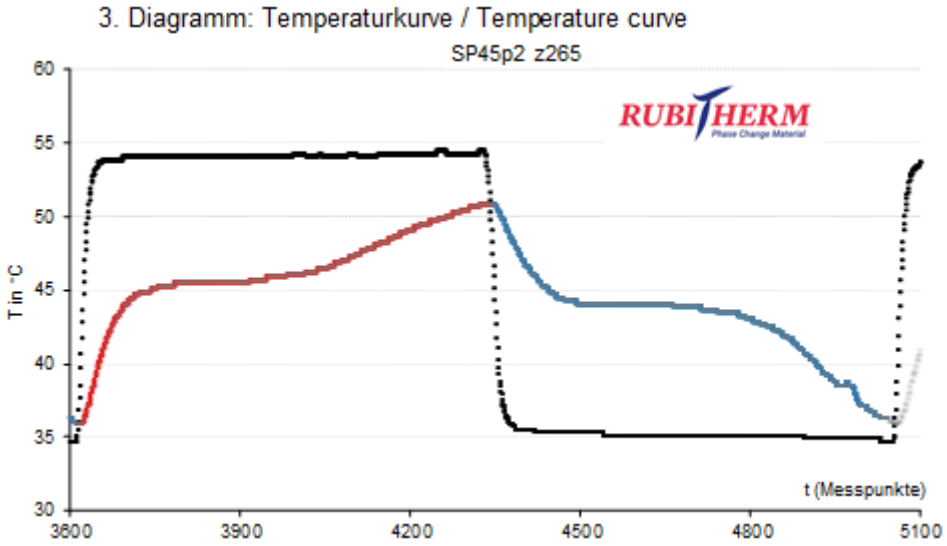

Figure 20: temperature curve of SP45p2 after 265 cycles

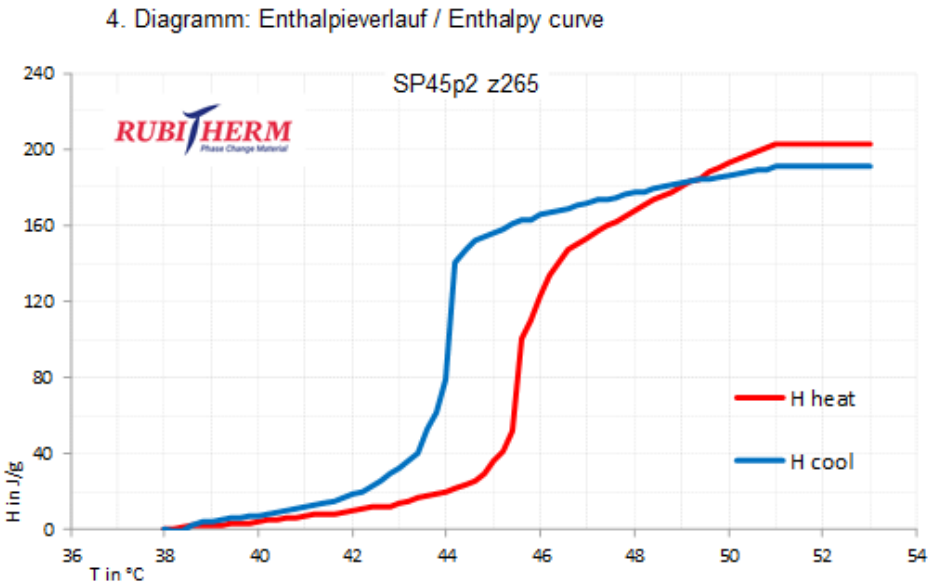

Figure 21: enthalpy curve of SP45p2 after 265 cycles

After the General Assembly (GA) meeting in Dublin a change of the required temperature for the democase in Montserrat was decided. The new temperature is now 30-31°C. For this Rubitherm chose a PCM: SP31 that appears to fulfill most of the desired properties well. It is an inorganic PCM and the thermophysical data are listed in **Error! Reference source not found.** and shown in Figure 22, Figure 23 and Figure 24**Error! Reference source not found.**. Rubitherm will do further research and development, as well as intensive storage testing, in this temperature section due to its enormous potential in TES applications.

The measurements for thermal conductivities were possible to be performed at Rubitherm only for certain materials, the values of which, were then approximated for the other chemically similar candidates. For this, these values are only an estimation. To measure the heat

conductivity a heat wire is placed between two PCM samples. Applying an electric current causes a rise in temperature and this is inversely proportional to the thermal conductivity of the surrounding PCM. More information can be found in the final report of the KOKAP project (funding code: 03ET1463A-C)

KOKAP - Kosteneffiziente Kapselmaterialien für Phasenwechselmaterialien : Berichtszeitraum: 01.08.2017-31.01.2021[[3] .

Table 4. main thermophysical properties of possible PCM for temperature range 45°C & 31°C

properties	**SP41**	**SP45p2**	**SP31**
Melting area [°C]	41-42	46-47	31-33
Freezing area [°C]	40-39	44-43	28-30
Heat storage capacity [kJ/kg] [Wh/kg]; T.-range	125 / 45; 34°C-49°C	203 / 56; 38°C-53°C	210 / 58; 24°C-39°C
Specific heat capacity [kJ/kg*K]	2	2	2
Density solid [kg/l]	1.35	1.35	1.35
Density liquid [kg/l]	1.25	1.25	1.25
Max. Operation temperature [°C]	71	75	50
Biobased?	yes	yes	yes
Corrosion [-]	Corrosive effect on metals	corrosive effect on metals	corrosive effect on metals

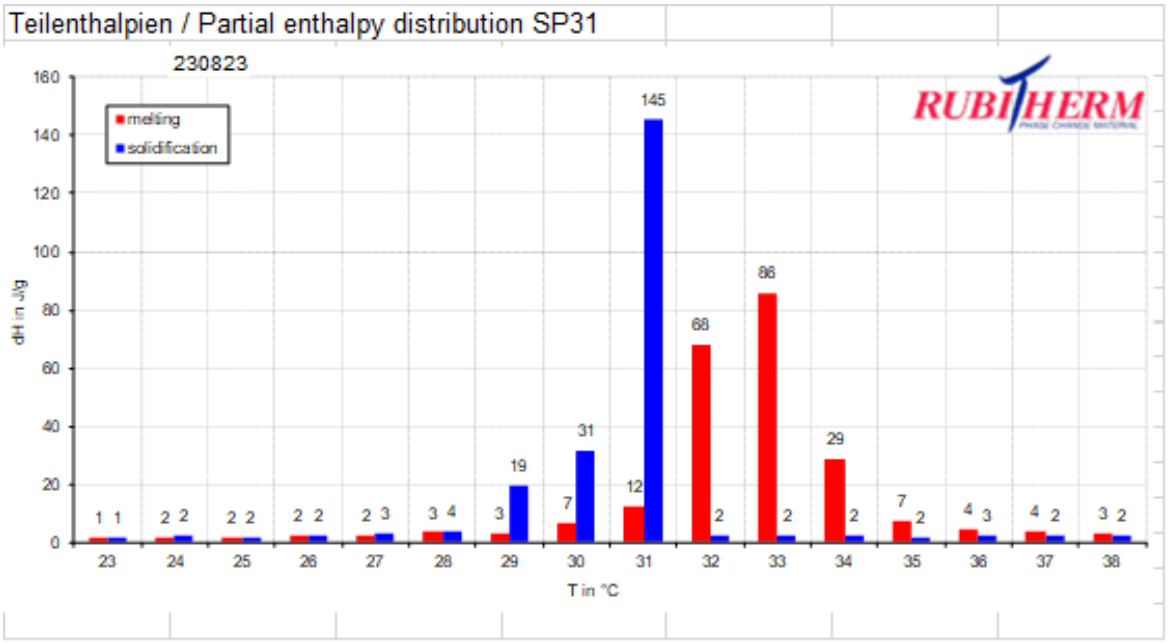

Figure 22: partial enthalpy of SP31

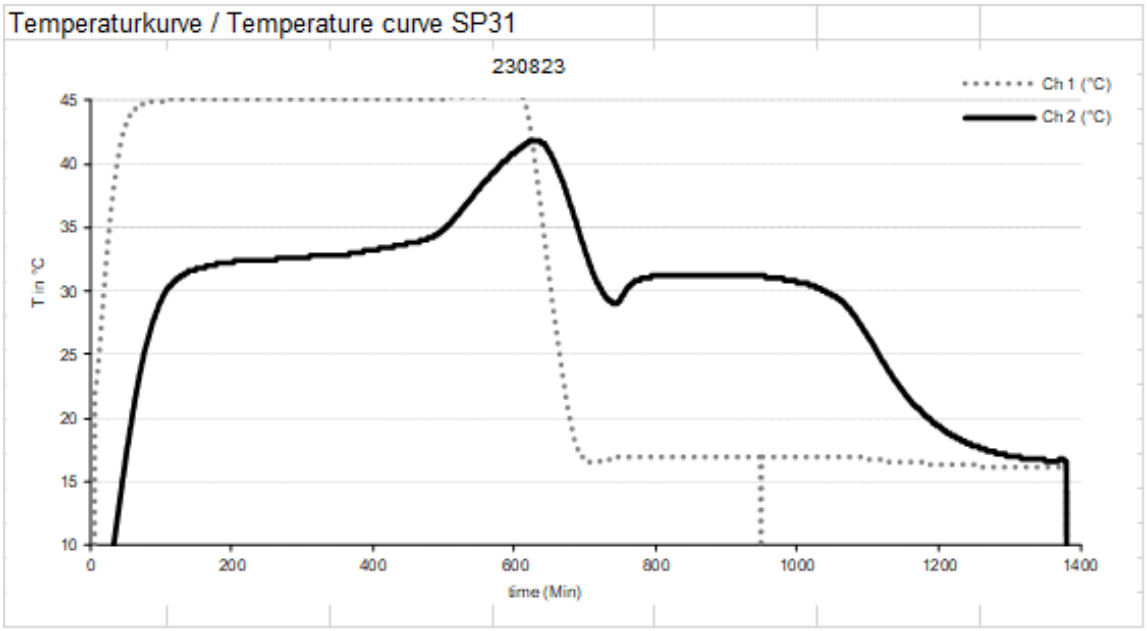

Figure 23: temperature curve of SP31

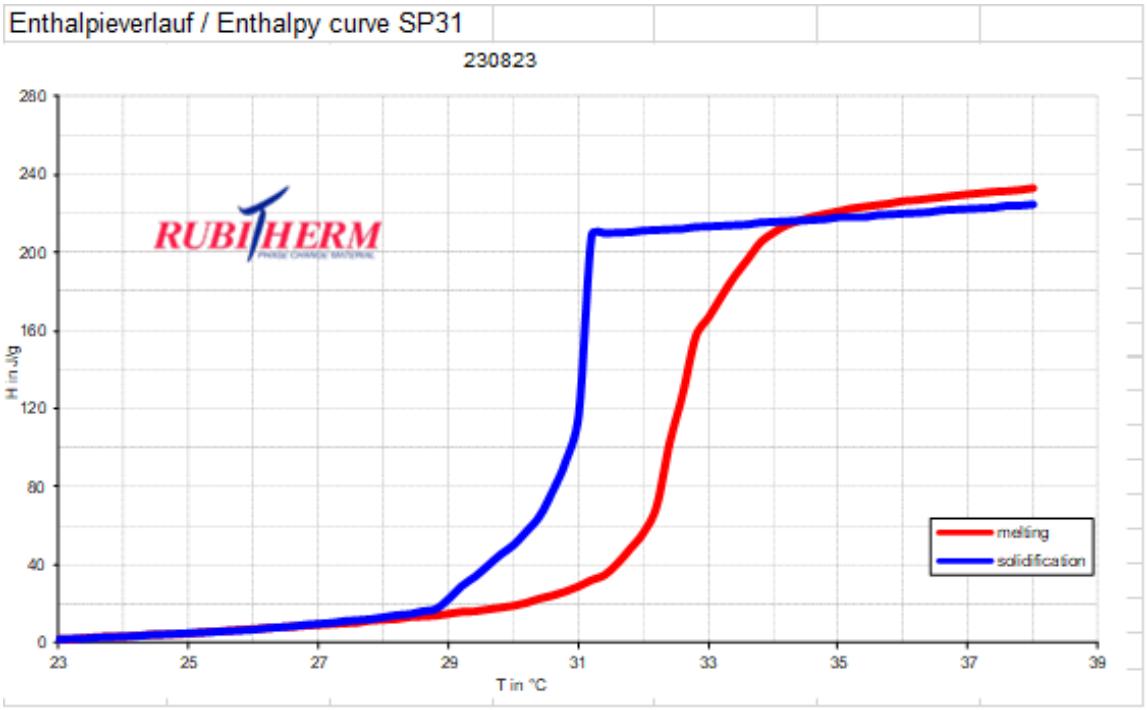

Figure 24: enthalpy curve of SP31

6.1.4. Calorimetric measurement – 30K range

Additional to the standard evaluation (of thermophysical properties) a wider range of 30K was evaluated for RT57HC and RT60HC. The gained diagrams are shown below in Figure 25 and Figure 26.

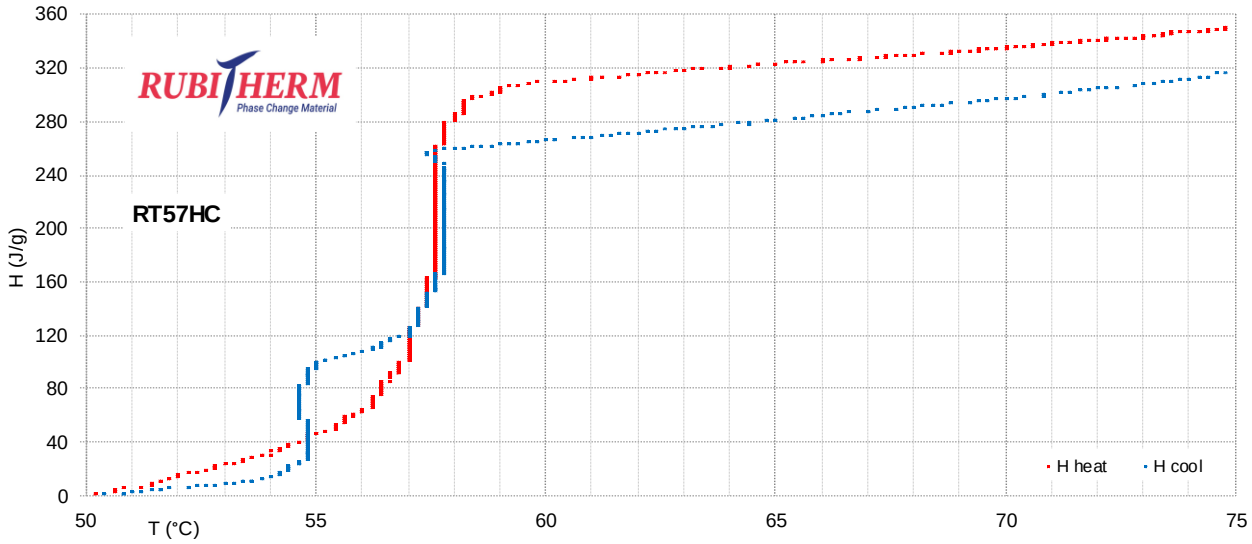

Figure 25: DSC-like enthalpy measurement of RT57HC

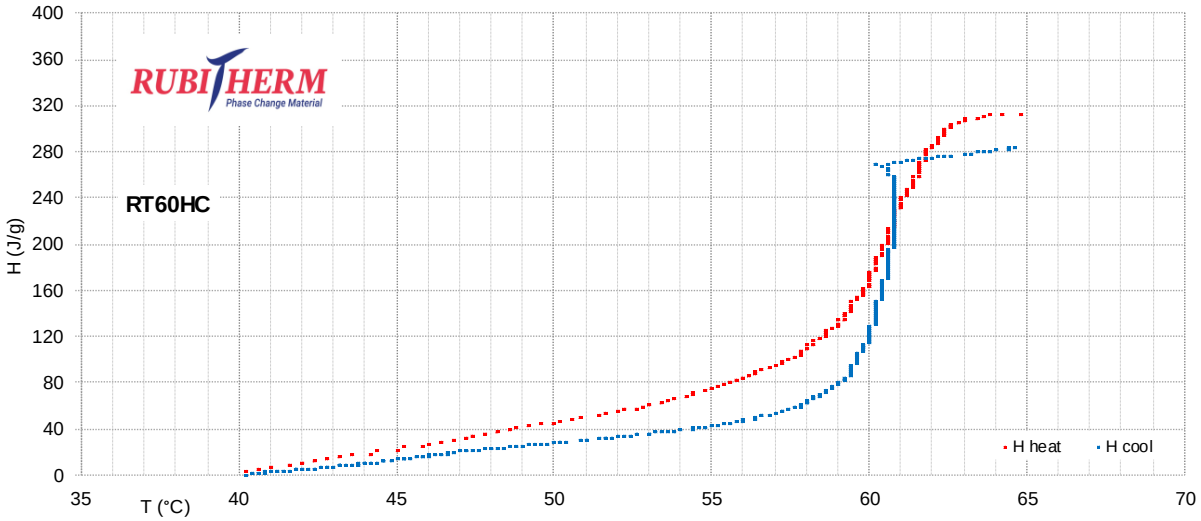

Figure 26: DSC-like enthalpy measurement of RT60HC

6.1.5. Corrosion tests at room temperature

For initial testing if the PCM is suitable with different metals, a room temperature corrosion test was performed by Rubitherm. Here, small pieces (10x10x1.5mm) of aluminum (heat exchanger material) and stainless steel (SS304 and SS316L; storage material) were first cleaned, dried and weighted before corrosion tests. After this, they were poured into the RT57HC and RT60HC in the liquid state. The formation of aluminum or iron oxide (white or brown layer) is a strong indicate for corrosion. The tests were done over 4 weeks at room temperature. After one month of testing the samples were removed, cleaned, and weighted again. Their results are discussed in section 6.2.1.

6.1.6. Corrosion tests at high temperature

Corrosion tests at high-temperature at KTH were performed (samples preparation and test itself) adhering to the relevant ASTM guidelines NACE TM169/G31-12a [3] and G1-03 (Reapproved 2017) [4]. Coupling these guidelines and available commercial dimensions of SS304 and SS316L, coupons of 10*10*1.5 mm3 dimensions were prepared for these corrosion tests. These were then scrubbed with household detergent paste (CIF [5]) using a polymeric cleaning mesh followed by thoroughly rinsing with water, ethanol and distilled water. Then the coupons were dried in an oven (Termarks TS4000) at 110 °C for ~12 hours and afterwards were kept desiccated for 24 hours at room temperature. The dimensions of all sides (using a Vernier caliper), the weights (using a Mettler Toledo XSR225DU Precision balance with 0.00001 g repeatability (d) in the measured range) and the photographs of each coupon were recorded before and after the corrosion tests.

Sufficient amounts (~1 liter each) of RT57HC and RT60HC, kept in separate beakers (covered with aluminum foil), were melted in an oven at 85 °C for ~12 hours. Glass bottles with polypropylene (PP) lids of 250 ml capacity, later used to pour these liquid PCMs, were also heated in the oven the same time (to avoid PCM solidification upon contact otherwise). These liquid PCMs were then poured into their designated glass bottles up to ~120 ml[2], one at a time.

For the corrosion tests, three coupons from each SS type were then inserted (one-by-one) into three marked designated bottles containing the intended liquid PCM (RT57HC and RT60HC respectively), e.g. as in Figure 27**Error! Reference source not found.** (a) and (b). Three coupons from each SS type were kept in liquid PCM of each type. These 12 bottles (3 coupons for each SS type and each PCM type) were then maintained at 85 °C in the same oven for 30 consecutive days. Additionally, two control coupons from the two SS types were kept in ambient conditions without any PCM, as shown in Figure 27 (c) and (d).

At the end of the corrosion tests, these coupons were cleaned thoroughly, step-by-step, first with hot water[3] and then with the polymeric mesh and detergent and CIF, followed by through rinsing with water and distilled water. Afterwards, upon rigorous drying, their masses, dimensions and photographs were recorded again.

Moreover, a preliminary pH analysis was done using pH paper on samples of liquid PCM that underwent the corrosion test in-contact with SS coupons versus without SS coupons. The observations herein were later regarded as incomplete as the PCMs were understood to be hydrophobic. Nevertheless, these pH-paper observations were still recorded and are discussed in section 6.2.1

[2] To maintain a volume safely above the required minimum ratio of test solution volume to test specimen surface, which is 0.2 ml/mm^2

[3] although the PCMs were not water soluble, hot water helped to melt the PCM on the surfaces

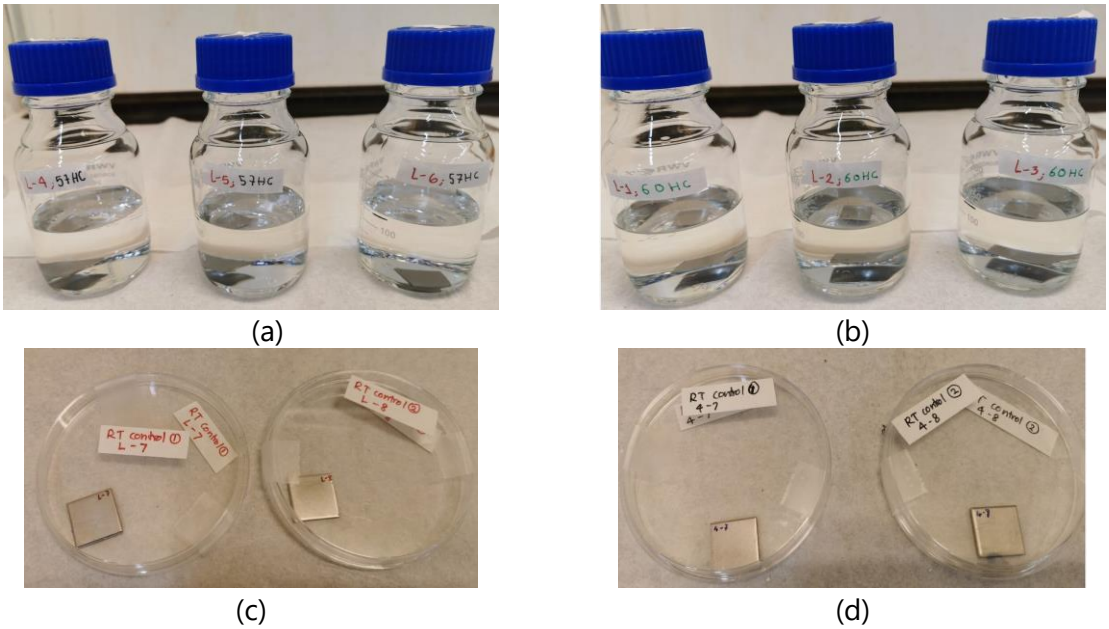

(a) (b)

(c) (d)

Figure 27. Corrosion tests preparation, just before start of test, e.g., showing (a) liquid RT 57HC and (b) liquid RT 60HC containing an SS 316L coupon each in the glass bottles with PP lids, and room-temperature control coupon samples from (c) SS 316 L and (d) SS 304.

6.1.7. Phase separation tests

The long-term stability tests were done with a 2m-high column. The PCM was filled inside, together with a small polymer heat exchanger. The PCM was then cycled in its given temperature range and if there is a possible separation, it can be seen through the column. This test indicates the segregation stability of salt hydrate PCMs.

6.1.8. Cycling testing

For measuring many cycles, a small sample of ~100g is prepared in a polypropylene or aluminium bag. It is then placed between temperature sensors on the bottom and a Peltier element on the top. The PCM can be heated and cooled with the aid of a control unit (see Figure 28). The data is recorded using a logger and can be evaluated after 100, 200, 1000 cycles. Characteristic cycling curves are then obtained as shown below in Figure 29.

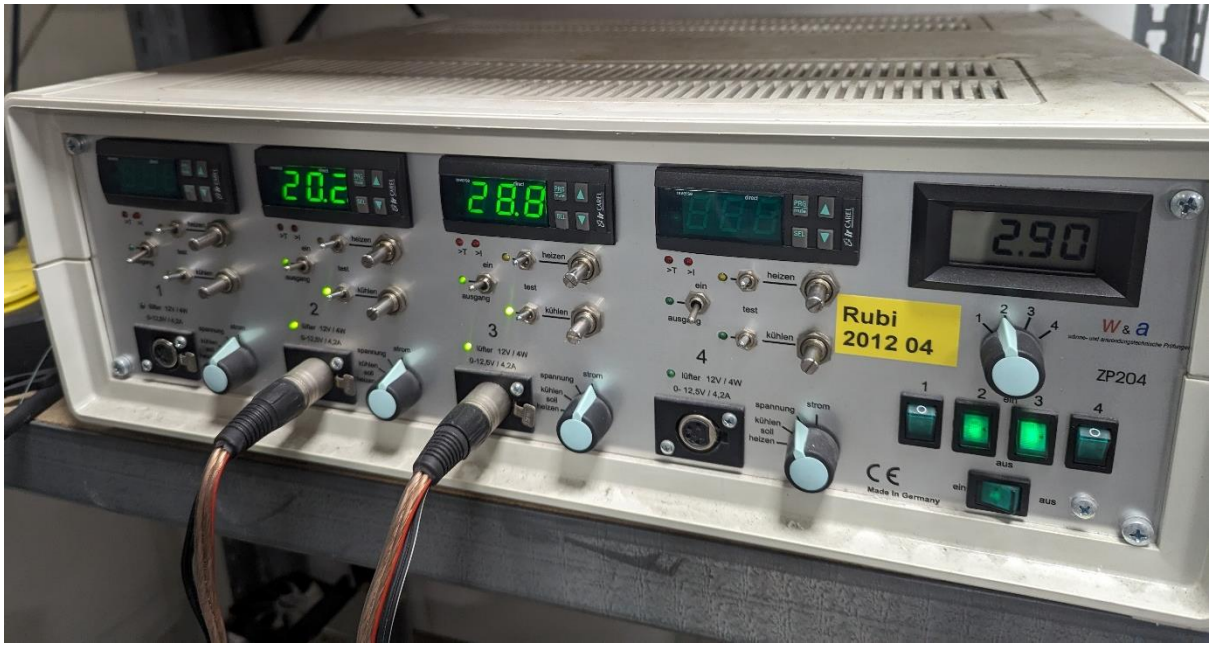

Figure 28: cyclic measurement control unit

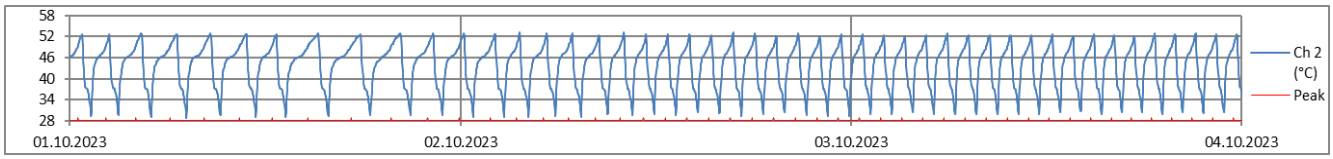

Figure 29: exemplary cyclic measurement of SP45p2

6.1.9. Solid and liquid state density

The densities of the short-listed two PCMs RT57HC and RT60HC (intended to assess for HYSTORE solutions I and III for space heating) were measured at both solid and liquid-states at KTH. Two stainless steel specific gravity cups (e.g. in Figure 30) of calibrated volume (50 ml and 100 ml respectively at 20 °C, i.e., at room temperature) from VWR [6] were used here.

Figure 30. The specific gravity (density) cups used [6]

First, the empty weights of each cup with and without the lid measured using a Mettler Toledo precision balance ME2002T (linearity 0.006 g and repeatability of 0.01 g) are summarized in Table 5.

Table 5. Specific gravity cups empty weights

Weight category	50 ml cup: Weight (g)	100 ml cup: Weight (g)
Cup alone	86.94	140.1
Lid	59.17	57.22
Cup total (with lid)	**146.11**	**197.32**

To also measure the liquid-state density, these specific gravity cups along with their lids were heated in an oven to 85 °C alongside ~100 ml of RT60HC and ~150 ml of RT57HC in separate beakers. Allowing sufficient time (~5 hours) for the PCMs to completely melt, these were quickly taken out of the oven, poured in respectively to the designated cup (RT60HC to 50 ml and RT57HC to 100 ml), and then the lids were placed on top to 'vent' excess volume. Their weights were then quickly measured (while the PCM is in liquid state). Then after, the cups with PCM were left for cooling at room temperature. After ~ 12 hours of cooling, the PCMs in the cups have solidified and had also slightly shrunk. Therefore, some more liquid PCM (till then retained in the oven at 85 °C) was then carefully poured into the designated cup, to fill the small gaps. Upon further cooling and solidification at room temperature for another 2 hours (c.f. , Figure 30) the weights of each solid PCM in the specific gravity cup were measured again.

(a) **(b)**

Figure 31. The specific gravity (density) cups filled with solid PCMs, (a) RT60HC in 50 ml cup and (b) RT57HC in 100 ml cup

By deducting the weight of the empty cup from the weight of the cup with PCM, respectively in liquid and solid state, the corresponding mass of PCM in each state can be obtained. Then for solid-state density, the solid PCM mass was divided by the calibrated volume (50.000 ml and 100.000 ml for RT60HC and RT57HC, respectively). For the liquid-state density, the cup's volume at 20 °C was adjusted to 80 °C (assuming the PCM cooled ~5 °C during the sample preparation process, once taken out from the oven). Using thermal expansion of stainless steel (assuming austenitic type) of 0.0000163 K^{-1} [7] into the volume of the cups (of a regular cylinder) at 80 °C were estimated. The liquid PCM masses were divided by these volumes, despite this volume change was then found to be negligible (only changes below 10 decimals).

These measured weights and final densities are presented in section 6.2.1, under Solid and Liquid state densities of RT57HC and RT60HC.

6.2. Results and Discussion - Intrinsic Property Characterization

In this section the results are presented. All obtained and determined values and data are listed in tables.

6.2.1. Material Intrinsic properties of the analysed PCMs

Solid and liquid state densities of RT60HC and RT57HC

The volumes of the two specific gravity cups, the masses of each PCM respectively at solid and liquid state, and therein their final densities are summarized in Table 6.

Table 6. Density measurements – intermediate data and final densities for RT57HC and RT60HC

Parameter	RT57HC, solid	RT57HC, liquid	RT60HC, solid	RT60HC, liquid
Cup Volume (cm^3) at 20 °C	100.000	--	50.000	--
Cup volume (cm^3) at 80 °C	--	100.000	--	50.000
PCM mass (g)	88.96	80.88	44.23	41.01
PCM density (kg/m^3)	889.6	808.8	884.6	820.2

Therefore, it seems that the density and hence volumetric change between solid and liquid states (20- 80 °C) of RT57HC and RT60HC are respectively about 9% and 7%.

6.2.1. Corrosion tests

After one month of room-temperature corrosion testing (conducted at Rubitherm) of RT57HC and RT60HC in contact with SS304 and SS316L, there was no changes in sample mass or surface. Therefore, it can be deduced that at room temperature, these PCMs have no corrosive behavior against these metals.

The high-temperature corrosion tests (conducted at KTH) on both SS304 and SS316L coupons yielded no noticeable mass, dimension or appearance changes in the coupons kept in contact with molten RT57Hc and RT60HC respectively at 85 °C for 30 consecutive days. These PCM samples also visually did not display any discoloration from initial to end states. The dimensions and masses of these SS coupons are presented in Table 7, Table 8, Table 9 and Table 10, for before and after tests. These measurements also confirm that there is no change in these coupons after corrosion tests.

Table 7. Initial (before test) dimensions and weights SS304 coupons (1-8)

Sample	Length of each side (cm)				width1 (cm)	width2(cm)	width3(cm)	weight (g)
4--1	2.01	2.01	1.99	1.99	0.13	0.14	0.135	4.445
4--2	2	1.995	2.01	1.99	0.14	0.135	0.14	4.501
4--3	1.99	2	1.99	1.975	0.135	0.135	0.135	4.497
4--4	1.99	2.055	2.01	2.08	0.14	0.135	0.14	4.75
4--5	2	2.04	2	2	0.14	0.145	0.14	4.575
4--6	2	2.02	2.01	2.02	0.14	0.14	0.14	4.555
4--7	1.98	2	2	1.99	0.135	0.14	0.14	4.481
4--8	2.02	2	2.025	2.025	0.14	0.135	0.14	4.572

Table 8. Final (after-test) dimensions and weights SS304 coupons (1-8). (7 and 8: control samples kept at room temperature, with no PCM, and hence no re-cleaning done)

								After hot water cleaning	After mesh cleaning
Sample	Length of each side (cm)				width1 (cm)	width2 (cm)	width3 (cm)	weight (g)	weight (g)
4--1	2.01	2.01	2.005	1.99	0.135	0.135	0.135	4.448	4.445
4--2	2.01	1.995	2.01	1.99	0.14	0.14	0.14	4.501	4.500
4--3	1.995	2	1.99	1.985	0.14	0.135	0.135	4.497	4.497
4--4	2.02	2.06	2.01	2.08	0.14	0.135	0.14	4.75	4.750
4--5	2	2.03	2.01	1.99	0.14	0.145	0.14	4.764	4.578
4--6	2.03	2.02	2.01	2.02	0.135	0.14	0.14	4.556	4.555
4--7	1.98	1.99	1.995	1.99	0.135	0.14	0.14	4.481	
4--8	2.01	2	2.025	2.025	0.14	0.135	0.135	4.572	

Table 9. Initial (before test) dimensions and weights SS316L coupons (1-8)

Sample	Length of each side (cm)				width1 (cm)	width2 (cm)	width3 (cm)	weight (g)
L--1	1.99	1.98	2.02	1.99	0.14	0.14	0.14	4.65
L--2	1.99	2	1.98	2.015	0.135	0.135	0.135	4.647
L--3	2.02	1.98	2.01	2	0.135	0.14	0.14	4.699
L--4	1.98	2	1.985	2.015	0.135	0.14	0.14	4.655
L--5	2.005	2	2	1.99	0.14	0.14	0.14	4.56
L--6	2	1.99	2.025	1.995	0.14	0.14	0.145	4.659
L--7	2	2.03	1.99	2.035	0.14	0.145	0.135	4.647
L--8	1.98	1.98	1.985	1.99	0.14	0.14	0.14	4.638

Table 10. Final (after-test) dimensions and weights SS304 coupons (1-8). (7 and 8: control samples kept at room temperature, with no PCM, and hence no re-cleaning done)

								After hot water cleaning	After mesh cleaning
Sample	**Length of each side (cm)**				**width1 (cm)**	**width2 (cm)**	**width3 (cm)**	**weight (g)**	**weight (g)**
L--1	1.99	1.99	2.02	1.995	0.14	0.14	0.14	4.65	4.649
L--2	1.99	1.995	1.98	2.015	0.14	0.135	0.14	4.648	4.647
L--3	2.02	2.01	2.015	2.03	0.15	0.14	0.14	4.698	4.697
L--4	2.01	1.995	1.99	2.01	0.14	0.14	0.14	4.655	4.655
L--5	2.005	2.01	1.99	1.985	0.14	0.14	0.14	4.559	4.557
L--6	2.005	1.99	2.025	1.995	0.14	0.14	0.14	4.653	4.655
L--7	2	2.01	1.99	2.035	0.14	0.145	0.135	4.647	
L--8	1.98	1.98	1.985	1.99	0.14	0.145	0.14	4.64	

The pH of the PCM samples (both RT57HC and RT60HC) that contained the SS coupons versus that did not contain any metal coupons was investigated after maintaining 30 days at 85 °C. Some representative examples of these observations are summarized in Figure 32 and Figure 33. RT60HC did not display any color change of the pH paper regardless of whether it was in contact with metal coupons (SS304 and SS316L) or not. This color matches the pH indication of 5, as seen in Figure 32, (a)-(c). RT57HC, on the other hand, indicated a shift in pH color towards a more acidic range (i.e., pH 3) in the samples that were in contact with both types of metal coupons, versus without any metal (showing a pH of 5).

(a)

(b)

(c)

(d)

Figure 32. Examples of the pH indications observed for RT60HC which had (a) no metal coupons, (b) an SS304 coupon and (c) an SS316L coupon (all with pH ~5), and also in (d) the color of the PCM after test (showing no noticeable change)

(a)

(b)

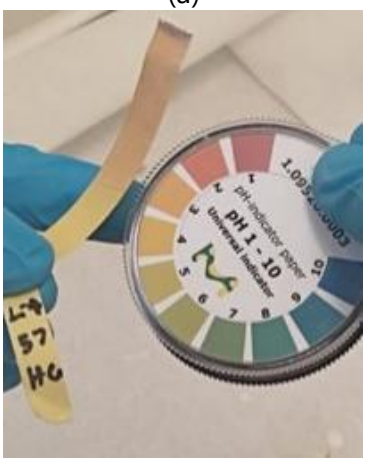

(c)

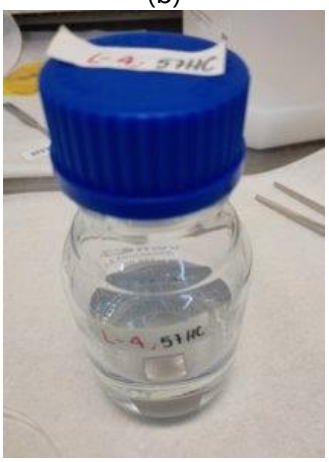

(d)

Figure 33. Examples of the pH indications observed for RT57HC which had (a) no metal coupons (pH ~5), (b) an SS304 coupon (pH~3) and (c) an SS316L coupon (pH~3), and also in (d) the color of the PCM after test (showing no noticeable change)

As explained in section 6.1.6, it was decided that these pH indications however are not entirely valid as both the PCMs are hydrophobic and hence would not properly respond to pH papers. Nevertheless, the color changes in RT57HC when in contact with both SS304 and SS316L was

here chosen as a decisive factor, particularly as the color indication pointed a change towards an acidic state. Therefore, it was decided RT60HC, although has a bit lower storage capacity, is the better alternative of the two PCMs for both HYSTORE solutions I and III, potentially providing more long-term stability in contact with both these metals.

6.2.2. Initial pre-selected list of PCMs

The summary of the above-discussed initial pre-selection of PCMs for HYSTORE solutions for 55-65°C temperature range, with their thermal properties, are summarized in Table 11.

Table 11. Main thermophysical properties of possible PCM for temperature range 55-65°C

properties	**RT57HC**	**RT60**	**RT60HC**	**RT62HC**	**RT64HC**	**SP58**
Melting area [°C]	57-58	55-61	58-61	62-63	63-65	56-59
Congealing area [°C]	57-56	61-55	60-58	62	64-61	56-54
Heat storage capacity [kJ/kg] [Wh/kg]; T.-range	230/63; 50°C-65°C	160/40; 53°C-68°C	210/58; 53°C-68°C	230/64; 55°C-70°C	250/70; 57°C-72°C	250/69; 51°C-66°C
Specific heat capacity [kJ/kg*K]	2	2	2	2	2	2
Density solid [kg/l]	0.99	0.88	0.85	0.99	0.88	1.3
Density liquid [kg/l]	0.85	0.77	0.75	0.85	0.78	1.2
Max. Operation temperature [°C]	85	80	90	90	95	85
Biobased?	yes	no	yes	yes	yes	yes
Corrosion [-]	No corrosive effect on metals	No corrosive effect on metals	No corrosive effect on metals	Slight corrosive effect on metals	No corrosive effect on metals	corrosive effect on metals

6.3. Concluding Remarks- Intrinsic Property Characterization

From the evaluation of the results here as a whole, it can be concluded that RT60HC is the optimal candidate PCM at the pre-selection level, for HYSTORE solution I. While RT57HC shows a second temperature peak/plateau at 54°C, RT60HC has only one sharp peak and a high storage capacity. It also fits with all the other requirements given in table 1. Besides, a slight doubt arose on RT57HC during the corrosion tests on SS304 and SS316L based on an 'approximate' pH analysis, yielding a tendency to become more acidic. However, as the pH

papers were then decided as unsuitable to measure the pH of these hydrophobic PCMs, this is merely a preliminary observation that needs further more valid investigations to verify.

For solution II it was decided to select SP31 as the most promising candidate also at this pre-selection level, for the demo-case in Montserrat. It is already a well-tested PCM from Rubitherm. SP31 has a high storage capacity, fits the temperature range of the given requirements, is non-corrosive against polymer HEX and is biobased.

The investigated properties of PCMs in the temperature range 40-45°C indicate that the following PCMs are the promising candidates: RT8HC, SP12sk and SP31. First results show a high storage capacity and non-corrosivity against polymers. RT8HC is already widely applied in cold chain logistics and air conditioning applications and has proved long term stability. [4] known to show no corrosion effects with aluminium and can therefore be recommended for the cooling application for solution I. The cycle stability is tested for 256 cycles for now and is still ongoing. Phase separation tests will be done in the future. Further storage testing and evaluation of data are planned for 2024.

Short-list of PCMs

The short-listed PCMs at this initial screening are summarized below in **Error! Reference s ource not found.**, **Error! Reference source not found.** and **Error! Reference source not found.** with their key properties. The relevant links are found in Appendix A- Material Safety Data Sheets (MSDSs) for those available.

6.3.1. Solution I: PCM ALL-IN-ONE

Table 12. short list of PCMs for solution I

PCM	Corrosion vs. stainless steel	Corrosion vs Aluminum	Heat storage capacity [J/g]	Melting T. [°C]	Congealing T. [°C]
RT8HC	No	No	190	7-9	8-7
RT60HC	No	No	210	58-61	60-58

Solution I and II cooling

6.3.2. Solution II: LOW-TEMP. HEATING & COOLING

[4] Zhang, X., Shi, Q., Luo, L., Fan, Y., Wang, Q., & Jia, G. (2021). Research Progress on the Phase Change Materials for Cold Thermal Energy Storage. Energies, 14(24), 8233.
Iskandar, S. H., Cofré-Toledo, J., Cataño, F. A., Ortega-Aguilera, R., & Vasco, D. A. (2023). Experimental study of the unconstrained melting of a phase change material for air-conditioning applications. International Journal of Refrigeration, 153, 19-32.

Table 13. short list of PCMs for solution II

PCM	Corrosion vs. stainless steel	Corrosion vs Aluminum	Corrosion vs. polymer	Heat storage capacity [J/g]	Melting T. [°C]	Congealing T. [°C]
RT8HC	No	No	Yes	190	7-9	8-7
SP12sk	Yes	Yes	No	160	12-13	11-10
SP31	Yes	Yes	No	210	31-33	30-28

6.3.3. Solution III: PCM HEATING

Table 14. short list of PCMs for solution III

PCM	Corrosion vs. stainless steel	Corrosion vs Aluminum	Heat storage capacity [J/g]	Melting T. [°C]	Congealing T. [°C]
RT60HC	No	No	210	58-61	60-58
RT57HC	No	No	230	57-58	57-56

7. High density PCM physical property testing

This section presents the high-density PCM property testing performed under real application conditions as relevant for HYSTORE solutions I and III. Potential high TES density PCMs, among other design criteria, were shortlisted from a number of PCM alternatives in the previous steps (by RUBI together with AIT and KTH), as in Section 6. From these, for the PCMs meant for heating applications, the real application conditions are achieved primarily by employing a bench-scale LHTES system at KTH, made of a shell-and-tube HEX with ~44 l PCM volume[5]. The chosen PCMs for heating applications were thermally cycled in this LHTES for similar operating conditions and their properties were analyzed at KTH. These tests and their results are presented and discussed here.

7.1. Materials and Methods- Bench-scale PCM Testing

The short-listed materials from initial screening (section 6) aiming for HYSTORE solutions I and III for space heating applications, and the corresponding bench-scale testing and data analysis method are explained here.

7.1.1. Materials

The shortlisted PCMs from T2.1 as described in section 6.3 that were considered for PCM heating solutions are the RUBI PCMs: RT57HC, RT60, RT60HC, RT62HC and RT64HC. These are all bio-based, except for RT60, thus giving priority on one overall criteria aimed in HYSTORE project, to employ renewable TES materials. Their final key attributes that dictated their suitability for the bench-scale LHTES testing are summarized in Table 15.

Table 15. Short-listed PCM candidates from RUBI considered for bench-scale testing selection

PCM	Corrosion of		Storage capacity (kJ/kg)	Phase change temperature range (°C)
	Stainless steel (SS)	Aluminium (Al)		
RT57HC	No	No	230	53-59
RT60*	No	No	160	55-61
RT60HC	No	No	210	58-61
RT62HC	No	Yes	230	62-63
RT64HC	No	No	250	63-65

*non-biobased

For cooling applications, the cycling stability tests of the three selected candidates (RT8HC, SP12sk and SP31) for HYSTORE solutions I and III are still ongoing, and will be reported in D2.1.

[5] At room temperature

Considering the space heating operating conditions for solutions I and III (c.f. Table 1), and the bench-scale LHTES system's materials of construction (i.e., stainless steel (SS) of types SS304 and SS316L), RT57HC and RT60HC were selected to be tested at KTH.

7.1.2. Bench-scale LHTES set-up and the long-term cycling tests

Error! Reference source not found. Error! Reference source not found.pictures the thermal en ergy storage unit for solution II LOW TEMP COOLING. The dimensions of the storage are 350x420x1200 mm. The storage material consists of plexiglass and a metal bracing for additional stability. An aluminum heat exchanger is located on the inside. For internal testing the storage was first filled with RT8HC. There are also water connections for easy installation on the top of the storage.

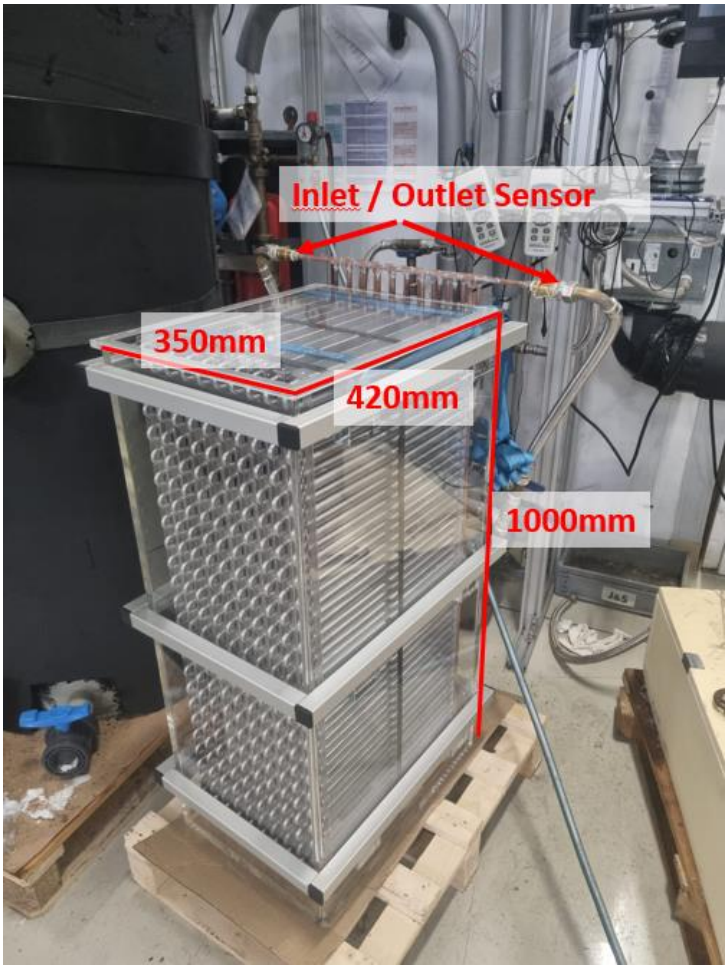

Figure 34: thermal energy storage with aluminum heat exchanger

In **Error! Reference source not found.** the inlet and outlet temperature of the TES is shown. I t is charged with ~3°C for 2 h 40 min. After this the discharging process started with 15-16 °C over 1h 40min. The diagram shows a relatively constant outlet temperature plateau at the phase change temperature of 8°C for RT8HC. The data was measured with the Comark N2014 data logger. The connected temperature sensor is a type K

In **Error! Reference source not found.** you can see the power and capacity of the RT8HC TES. T he maximum capacity of this 220-liter storage (~180 liter PCM) is 5.1 kWh at its peak of charging. The TES discharges very quickly, which indicates that the heat exchanger has very good thermal conductivity.

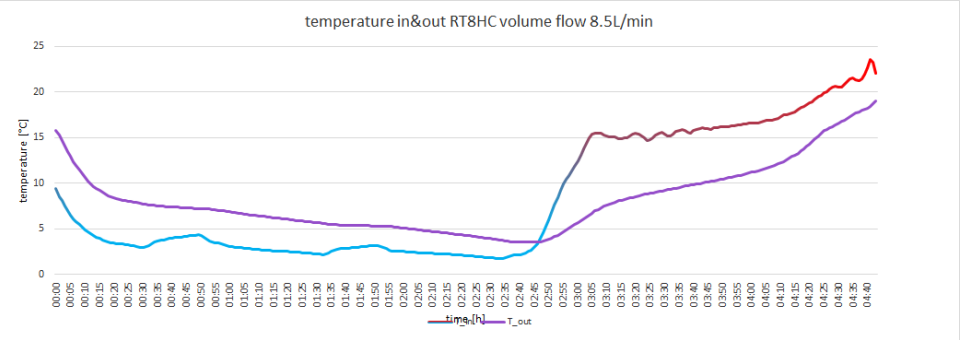

Figure 35: in and out temperature of the TES with aluminum HEX; RT8HC

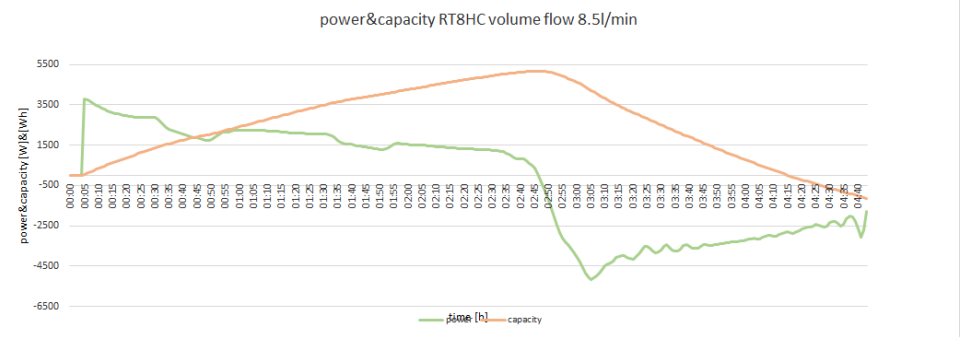

Figure 36: power and capacity of the TES with aluminum HEX; RT8HC

The schematic of the bench-scale LHTES system at KTH is shown in Figure 37, with its components detailed in Table 16 and Figure 38 depicting the real system. Figure 38 labels most of its components and points, except for the buffer tank which is located underneath the LHTES bench, and PCM outlet at the left-hand side bottom part of the LHTES unit (not visible in the figure).

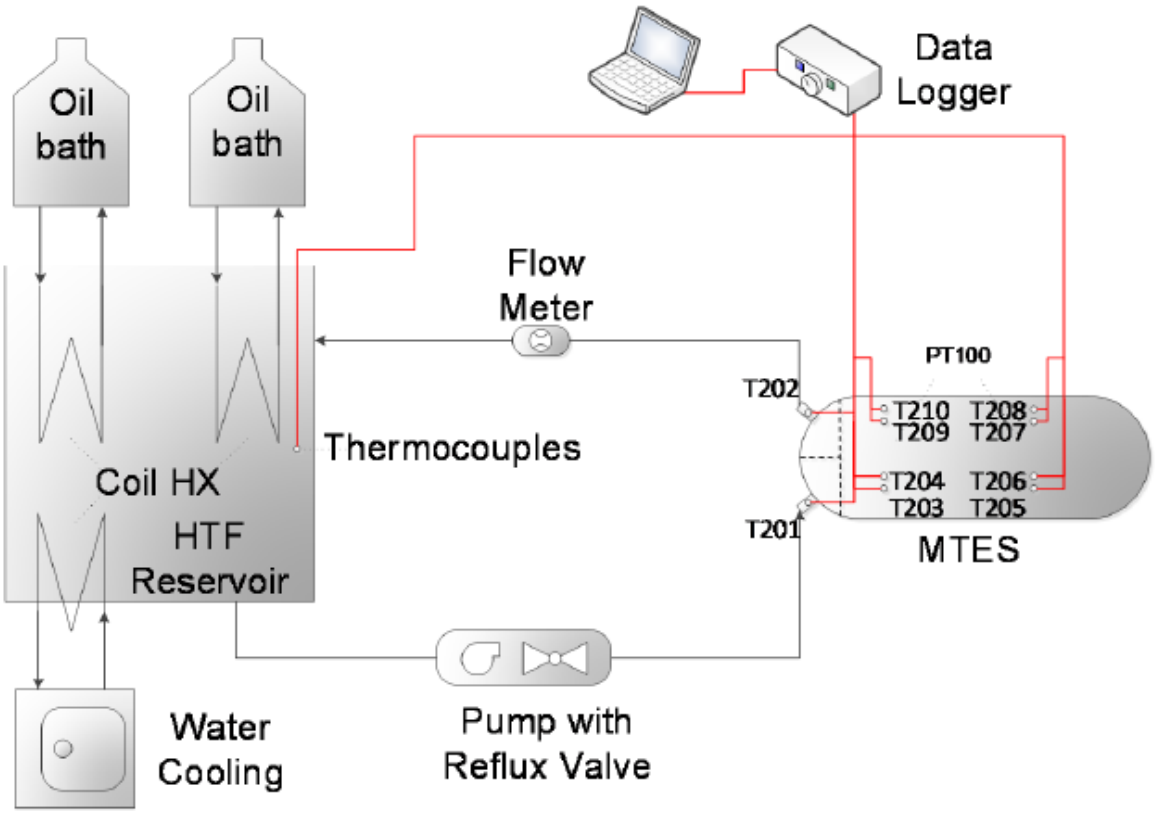

Figure 37. Schematic of the Bench-scale LHTES system set-up Adapted from [8], [9])

Table 16: KTH- LHTES system components details [8]

Component	**Description**
Oil reservoir	Container for the heat transfer fluid (i.e., a thermal oil)
Cycloidal gear pump with reflux valve	Pumps heat transfer fluid from the oil reservoir to the tank
LHTES tank	Shell and tube heat exchanger which holds the PCM on the shell side, while letting it being heated up by the oil running on the tube side
Positive displacement flow meter	Measures the flow of oil which the pump is delivering
PT100s & thermocouples	Temperature measuring equipment
Temperature converter	Device converting the information given by the PT100s to a temperature input data into computer
Thermostat oil baths	Heats up the oil to an appropriate temperature
Coil *Heat Exchanger* (*HEX*)	A closed loop which leads the heating/cooling fluids through the oil reservoir
Water sink	Provides water to cool down the oil
Insulation	Reduce heat losses and protects users

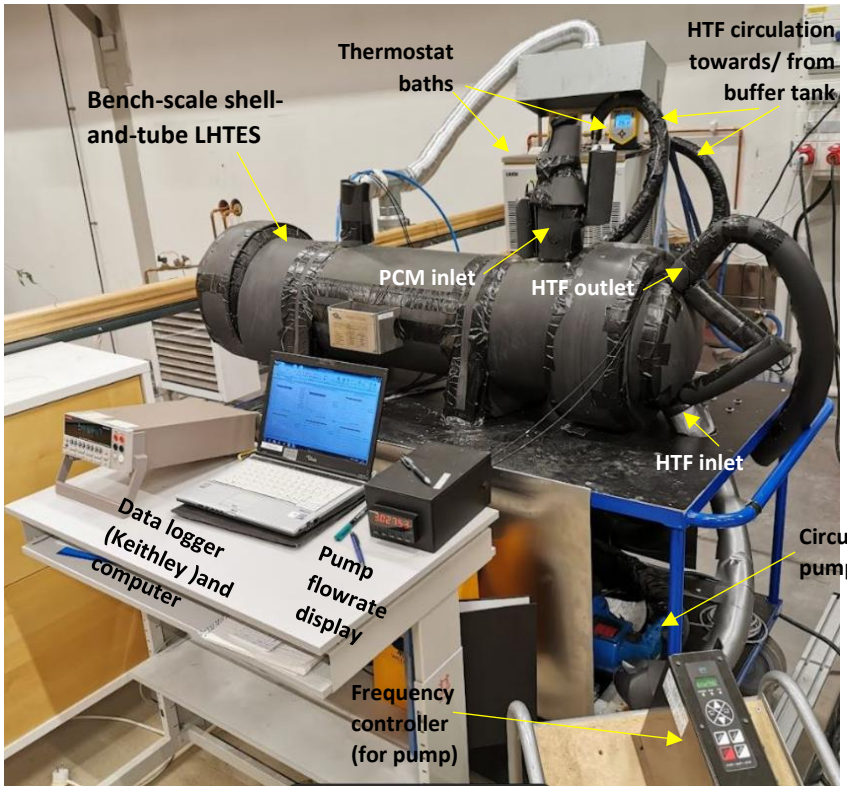

Figure 38: The LHTES system at KTH. (HTF: Heat transfer fluid)

As specified in Table 16, the LHTES unit comprises a shell-and-tube heat exchanger (HEX) configuration. In this, the shell contains the PCM and tubes carry the heat transfer fluid (HTF) which is Renolin THERM 300 X (a paraffin-based thermal oil) from FUCHS [10]. The internal configuration of this LHTES unit and the arrangement of temperature sensors (Resistance Temperature Detectors (RTDs) of PT 100 type) inside are shown in Figure 39.

Eight RTDs, 203, 204, 205, 206, 207, 208, 209 and 210 were placed in the left half of the LHTES cylinder (as shown in Figure 40), divided through a vertical plane A-A as in Figure 39 (a)). Two RTDs, 201 and 202 were also inserted respectively into HTF inlet and outlet. One T-type thermocouple 101 were also inserted into the HTF buffer tank. These thermal sensors' calibration data and depths of the thermal sensors placed inside the LHTES are found in e.g. [11]: Appendix 3.

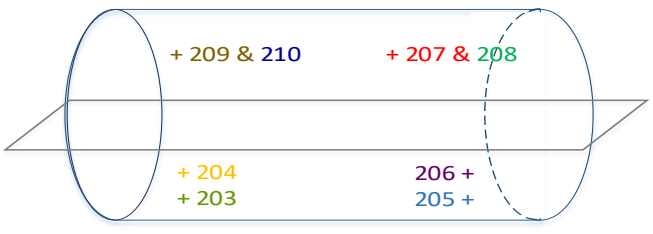

(b) horizontal cross-section

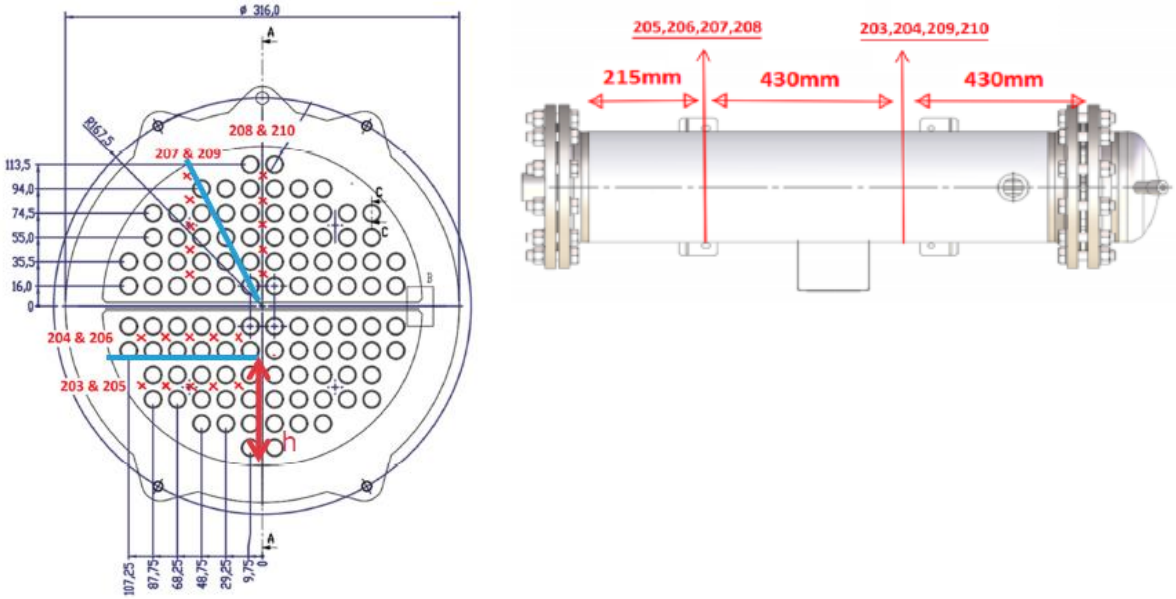

(a) vertical cross section *(c) dimensions*

Figure 39: Internal configuration, the arrangement of temperature sensors inside, and dimensions of the LHTES unit at KTH (reproduced with permission from [8], [11] and [9])

(a) 203 & 204

(b) 205 & 206

(c) 207 & 208

(d) 209 & 210

Figure 40. Thermal sensors placement in the LHTES, (a) 203 & 204, (b) 205 & 206, (c) 207 & 208 and (d) 209 and 210

Each PCM type (RT57HC followed by RT60HC) was respectively filled into 3 metallic Jerry Cans (of 20 L nominal volume) each, in the solid pelleted form, with respective weights measured (of empty and full cans). The PCMs in the cans were then melted in an oven maintained at 85 °C for ~12 hours. The liquid PCM was poured into the LHTES through PCM inlet (c.f. Figure 38) and the final weights of the Jerry cans were also recorded. Thereby, the final respective mass of PCMs poured into the LHTES were found to be 39.93 kg for RT57HC and 38.92 kg for RT60HC. The weighing balance used here is a Delta 5 (Svenska Våg AB) type, with a readability of 0.02 kg and maximum weight of 150 kg.

RT57HC was first tested in this bench-scale LHTES system for 27 consecutive heating/cooling cycles. Thereafter, the LHTES was rigorously cleaned (by flushing with distilled and de-ionized water multiple times (after maintaining the unit with water at 85 °C for 4-12 hours each time) and dried by maintaining the LHTES at 85 °C for ~2 days with PCM inlet and outlet open. Then the LHTES was filled with RT60HC and tested for 50+ (53) heating/cooling cycles[6]. The thermal program used in the thermostat baths was isothermal conditions at 30 °C to 95 °C, which resulted in around 35 °C to 85 °C in the HTF buffer tank supplying to the LHTES. The baths were maintained 16 hours at each isothermal step, meaning each heating and cooling cycle took 16 hours respectively.

The HTF flow through the LHTES was maintained always at 3 l/min, while the HTF inlet and the outlet temperatures were also measured (with channels 201 and 202 respectively).

Heat Transfer Fluid (HTF) Renolin Therm 300 X Properties

Renolin Therm 300 X is stated to have the typical properties as in Table 17 and with density and specific heat capacity changes with temperature, respectively as in Figure 41 and Figure 42. Particularly the density and specific heat capacity variations were considered in the HTF energy storage capacity calculations.

Table 17. Typical thermophysical properties of Renolin Therm 300 X [10]

Characteristics	Typical value	Unit	Method
Density at 15°C	875	kg/m^3	ISO 12185
Flash point COC*	235	°C	ISO 2592
Pour point	-24	°C	ISO 3016
Viscosity at 40°C	52.5	mm^2 / s	ISO 3104
Viscosity at 100°C	7.5	mm^2 / s	ISO 3104
Viscosity index	103	-	ISO 2909

*COC (Cleaveland Open Cup) [12]

[6] Within the available time and resources, it was decided to perform at least 25 heating/cooling cycles per PCM. With some of the results leaning more favourably towards RT60HC (than RT57HC), it was decided to allow more cycling within the task timeline, hence reaching 50+ cycles for that.

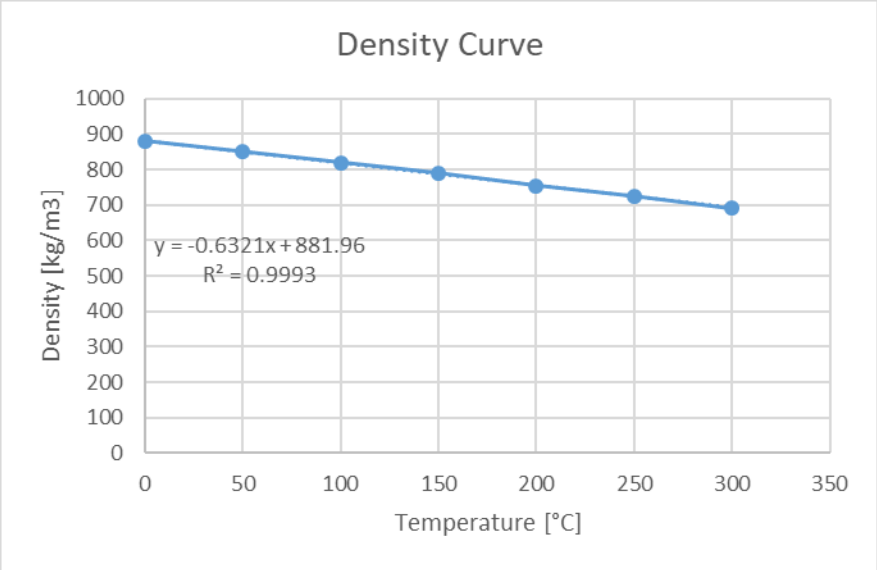

Figure 41. Renolin Therm 300 X (HTF) density variation with temperature (adapted from [10])

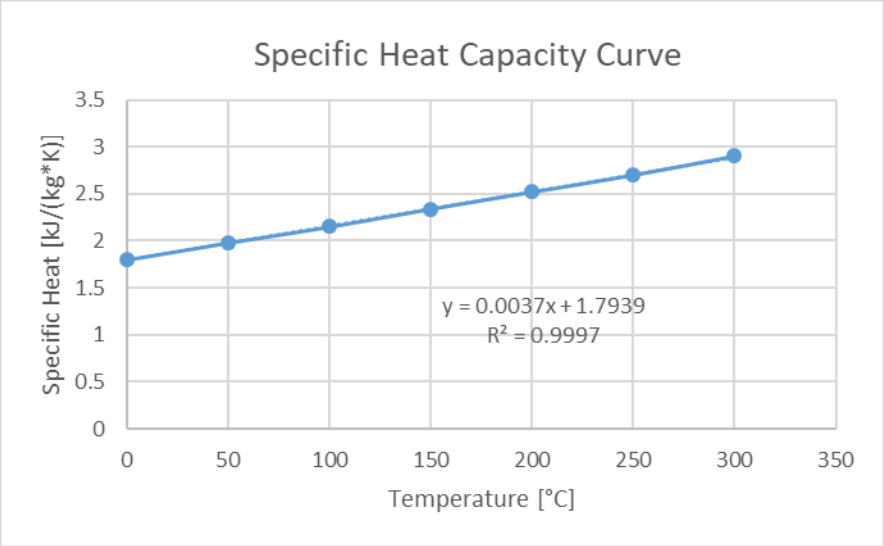

Figure 42. Renolin Therm 300 X (HTF) specific heat capacity variation with temperature (adapted from [10])

PCM thermal properties: RT57HC and RT60HC

The temperature range of 35 °C to 79 °C was considered in the data analysis for the energy storage property evaluation. The final thermal property data (phase change temperatures and enthalpies as well as specific heat capacities) for solid and liquid phases as respectively listed in Table 18 and Table 19 were used for RT57HC and RT60HC, compiled using the intrinsic property data from RUBI in section 6.2.1 and additional extended temperature-range tests that were also provided as complements. As RT57HC displays two phase changes, a solid-solid change and solid-liquid change, their specific heat capacities and latent heats are presented identifying these two solid phases as solid1 and solid2 in Table 19.

Table 18. RT57HC final thermal properties used

	Cooling		Heating	
	c_p / L	Temperature range (°C)	c_p / L	Temperature range (°C)
c_p,solid1 (kJ/(kg·°C))	**3.9**	35 - 54.5	**10.2**	35 – 56.6
Latent heat1 L1 (kJ/kg)	**82.5**	54.5 - 54.9	**197.5**	56.6 – 57.5
c_p,solid2 (kJ/(kg·°C))	**8.6**	54.9 - 56.9	**45**	57.5 – 57.9
Latent heat2 L2 (kJ/kg)	**142.5**	56.9 - 57.9	**20**	57.9 – 58.4
c_p,liquid (kJ/(kg·°C))	**3.3**	57.9 - 79	**2.9**	58.4 - 79

Table 19. RT60HC final thermal properties used

	Cooling		Heating	
	c_p / L	Temperature range (°C)	c_p / L	Temperature range (°C)
c_p,solid (kJ/(kg·°C))	**4.1**	35-57.5	**6.1**	35-57.8
c_p,liquid (kJ/(kg·°C))	**1.9**	62-79	**2.2**	62.5-79
Latent heat L (kJ/kg)	**205.0**	57.5-62	**200.0**	57.8-62.5

Energy capacity of the HTF

As a whole, by combining the temperature (of PCM and HTF) and flow rate (of HTF) measurements with their known properties (listed above), the TES capacities were calculated for the HTF (comparing inlet and outlet temperatures) and also the PCM respectively.

The heat delivered (during heating cycles) and absorbed (during cooling cycles) by the HTF was calculated using Equation 1 and Equation 2 [11] considering sensible heat transfer over 35 °C -79 °C range.

$$Q_{HTF} = \sum_{i=A}^{B} \int_{t_i}^{t_{i+1}} \dot{Q}_{HTF}\, dt \qquad \textit{Equation 1}$$

$$Q_{HTF} = \sum_{i=A}^{B} \int_{t_i}^{t_{i+1}} \rho_{T\,mean_{HTF}} \times \dot{v} \times c_{p\,mean_{HTF}} \times \left(T_{in,i} - T_{out,i}\right) dt \qquad \textit{Equation 2}$$

Where,

Q_{HTF}: Energy capacity in HTF (kJ)

A and *B*: the final time points between which the energy capacity is calculated (in a given heating or cooling cycle)

$\dot{v}$: HTF volumetric flowrate (m^3/s)

$\rho_{T\,mean_{HTF}}$: Density of HTF at the mean temperature between HTF inlet and outlet at time i (kg/m^3)

$c_{p_{T_{mean_{HTF}}}}$: Specific heat capacity of HTF at the mean temperature between HTF inlet and outlet at time i (kJ/(kg·K))

$T_{in,i}$ and $T_{out,i}$: inlet and outlet temperature of HTF at time *I* (°C)

Mass estimation for each of the 8 sensors inside LHTES

As the temperature distribution in the LHTES per sensor was not homogeneous, these were assigned certain portions of the PCM mass, considering a symmetric distribution along the blue lines in Figure 39 (a). Here, it was considered that the mass of PCM assigned to sensors 203, 204, 207 and 208 was similar to the mass assigned to respective sensors 205, 206, 209 and 210 [11]. These masses were estimated first considering the corresponding volume.

The volume assigned to sensors 203 and 204 (thus also 205 and 206) was calculated per Equation 3 for calculating a partially full cylinder volume [11].

$$V_{partial}(H) = L \times \left[r^2 \times \cos^{-1}\left(\frac{r-H}{r}\right) - (r-H) \times \sqrt{2 \times r \times H - H^2}\right] \quad \textit{Equation 3}$$

Where,

H: Considered (partial) height of the cylinder (m)

$V_{partial}(H)$: Cylinder partial volume at considered height *H* (m^3)

L: Cylinder length (m)

r: Cylinder radius (m)

The PCM volume assigned to sensor 207 (and thus also to 209) was estimated approximating it as corresponding to 1/3 of a half of the LHTES left-half volume. The volume assigned for sensor 208 (and thus 210) was then approximated to be corresponding a half of the volume on 207, i.e., taking up 1/6 of a half of the LHTES left-half volume [11].

The LHTES also contains the HTF tubes, the volume of which was excluded in the PCM volume calculations. This volume of the HTF tubes v_s (m^3) was estimated per Equation 4, with further details available in Maurel, 2017 [11].

$$v_s(N) = N \times \frac{L}{2} \times \pi \times \frac{d_0^2}{4} \quad \textit{Equation 4}$$

Where,

N: number of HTF tubes

d_0: HTF tubes' outer diameter (m)

The numerical sum of the assigned masses (by multiplying the obtained final volumes -minus the HTF tube volumes)- by the PCM density) into all 8 sensors can be found as slightly overestimated when compared with the real mass of PCM poured into the LHTES (in liquid state, filling the entire LHTES effective volume). To adjust this difference, a ratio γ_m was defined between the real total PCM mass (M, kg) versus the total estimated as assigned to the 8 sensors as a whole, as in Equation 5.

$$\gamma_m = \frac{2 \times M}{2 \times \sum_{s=203}^{s=210} m'_s}$$

Equation 5

Where, m'_s is the respective first estimated mass (kg) assigned per sensor. This respective m'_s was thus multiplied by γ_m to obtain the corrected mass per sensor. The final equations for the mass estimation per sensors are found in Maurel, 2017 [11]. The LHTES was first filled with liquid PCM, and then it is assumed to be completely full at liquid state. Thus, these mass assignment per sensor is valid for the liquid PCM. However, the density of the PCMs is different in liquid and solid state as presented in section 6.2.1. Then due to volume contraction in solid state, a small air-gap is inevitable to be at the top part of the LHTES cylinder, as conceptualized in Figure 43.

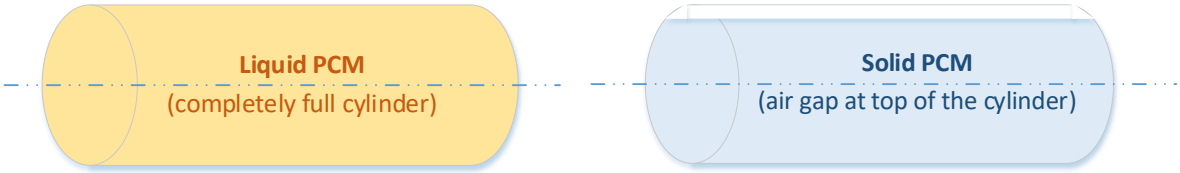

(a) Liquid PCM state **(b)** Solid PCM state

Figure 43. Differences in the PCM volume in the LHTES cylinder when it is in (a) liquid state and (b) solid state

The PCM mass measurements were done when the PCM is in liquid state, totaling to 39.93 kg for RT57HC and 38.92 kg for RT60HC. Based on their density data (section 6.2.1) it is found that in liquid state, their volumes are 49.4 l and 47.4 l, and in solid-state are 44.9 l and 44.0 l respectively. Thus, it appears that the solid PCM volume is what corresponds to the stated volume on the LHTES data plate, as ~44 l. These volumes and thus the corresponding mass differences in the upper and lower halves of the LHTES were also accounted when estimating the final masses for each sensor, then in solid-state. Namely, the lower half of the cylinder is full in both liquid and solid states, while the upper half of the volume is partially filled and is as listed in Table 20. This final volume for solid PCM was then used in estimating the portion of solid PCM assigned to each sensor in the upper half of the LHTES (i.e., 207, 208, 209 and 210) following the same procedure described the above.

Table 20. Final mass and volumes of RT 57HC and RT 60HC in LHTES in liquid and solid states, and in upper and lower halves (used for adjusting mass assigned for upper half of sensors in solid state)

	RT 57HC	**RT 60HC**
Total Mass (kg)	39.93	38.92
Total Liquid volume (L)	49.37	47.45
Total Solid volume (L)	44.89	44.00
Volume difference between liquid and solid (L)	4.48	3.45
Half of liquid volume =Solid volume in bottom half of LHTES cylinder (L)	24.68	23.73
Solid volume in the top half of LHTES cylinder (L)	20.20	20.27

Accordingly, the final masses of PCM estimated assigned to each sensor are listed in Table 21. As these 8 sensors are placed in only one half of the volume of the LHTES, the masses in Table 21 are multiplied by 2 to reach the total mass of PCM.

Table 21. Estimated respective mass of PCMs per sensor, for solid and liquid states

Sensors (respectively)	**Estimated mass** of **RT 57HC – liquid** (kg)	**Estimated mass** of **RT 60HC-liquid** (kg)
203 = 205	2.82	2.75
204 =206	2.17	2.11
207 = 209	3.32	3.23
208 = 210	1.67	1.63
Total on sensors	*19.97*	*19.46*
Sensors (respectively)	**Estimated mass** of **RT 57HC – solid** (kg)	**Estimated mass** of **RT 60HC-solid** (kg)
203 = 205	3.39	3.62
204 =206	2.60	2.78
207 = 209	2.66	2.22
208 = 210	1.34	1.12
Total on sensors	*19.97*	*19.46*

Energy storage capacity of the PCM in LHTES

The heat stored (during heating cycles) or released (during cooling cycles) by the PCM was calculated via Equation 6 and Equation 7 [11], considering both the sensible and latent heat capacity over the same 35 °C -79 °C range.

$$Q_{PCM} = \sum_{i=A}^{B} \dot{Q}_{PCM_i} \times 2 \quad \text{Equation 6}$$

$$\dot{Q}_{PCM_i} = \sum_{s=203}^{s=210} \{m_s \times [c_{p_{Tmean},i_{PCM,s}} + D(T_{mean(i;i+1),s}) \times \Delta h_{PC}] \times (T_{i+1,s} - T_{i,s})\} \quad \text{Equation 7}$$

Where,

S: respective sensor, 203, 204, 205, 206, 207, 208, 209 or 210

m_s : final corrected mass assigned per sensor (kg)

$T_{i+1,s}$ and $T_{i,s}$: temperature of PCM around a respective sensor at two consecutive time steps i and $i+1$ (°C)

$T_{mean(i;i+1),s}$: Mean temperature between consecutive time steps i and $i+1$ for a respective sensor (°C)

$c_{p_{Tmean},i_{PCM,s}}$: Specific heat capacity of PCM located around the respective sensor at time i corresponding to $T_{mean(i;i+1),s}$ (kJ/(kg·K))

Δh_{PC}: Phase change enthalpy (kJ/(kg) of the given phase change

Here, *D* is the adapted Dirac delta (or Heaviside) function defined by Chiu and Martin, 2011 [13] as in Equation 8 [11].

$$D(T) = \frac{1}{b \times \sqrt{\pi}} \times exp\left(-\frac{(T - T_{PC})^2}{b^2}\right)$$ *Equation 8*

Here, the parameter b is determined using the phase change temperature range T_{PC} (°C), by solving Equation 9 [11], [13].

$$\int_{T_{range\ PC1}}^{T_{range\ PC2}} D(T)dt = 0.99$$ *Equation 9*

The phase change temperature range T_{PC} (°C) was determined respectively for PCM heating (i.e., melting or charging) and cooling (i.e., freezing or discharging) cycles, and for each sensor. The phase change temperature was defined as the temperature inflection points at the start and end of the phase change plateau respectively. These were determined by using the cross-section temperature point of two tangents drawn on the plateau versus respectively the respective leading or receding sensible heat storage parts of the temperature-history (i.e., temperature versus time) curve for each sensor and phase [11]. Once the phase change start and end was identified for each sensor, the final phase change temperature range T_{PC} (°C) was determined by taking the mean of the start and end temperature ranges of all sensors (i.e., $T_{range\ PC1}$ and $T_{range\ PC2)}$ for that particular cycle, respectively. This is further explained along results in section **Error! Reference source not found.**. T_{PC} is then calculated per Equation 10 [11].

$$T_{PC} = T_{range\ PC1} + \frac{\Delta T_{range\ PC}}{2} = T_{range\ PC1} + \frac{T_{range\ PC2} - T_{range\ PC1}}{2}$$ *Equation 10*

As RT57HC displays two phase changes, the above detailed method was applied for each respective phase change, and then was combined with three different sensible heat storage segments (of the 2 solid phases and the liquid phase). For RT60HC, the procedure was directly applied.

Energy absorbed by the stainless-steel LHTES HEX

The empty LHTES unit (the cylinder, flanges and coupling so on) and the HTF tubes are made of stainless steel (types SS304 and SS316L) with a total weight of ~150 kg. This, referred to as SS_{HEX} as a whole, also absorbs a considerable amount of heat, which is calculated for the full temperature range 35 °C to 79 °C using Equation 11.

$$Q_{SS_{HEX}} = m_{SS_{HEX}} \times c_{p_{SS_{HEX}}} \times \Delta T$$ *Equation 11*

Where,

$Q_{SS_{HEX}}$: Heat absorbed by the LHTES unit and HEX (kJ)

$m_{SS_{HEX}}$: Total weight of the LHTES (empty) unit and HEX made of stainless steel (kg) = ~150 kg

$c_{p_{SS_{HEX}}}$: Specific heat capacity of stainless steel (kJ/(kg·K))

Using the specific heat of AISI SS 304, which is 0.5 kJ/(kg·K) [14] as a representative $c_{p_{SS_{HEX}}}$ estimation, the total energy stored in the LHTES SS_{HEX} is found to be 3300 kJ.

Energy Balance

Finally, the energy capacity of the HTF is compared to the energy storage capacity of LHTES, via energy balance analysis.

During the charging of LHTES (i.e., heating and thus melting the PCM), the heat supplied by the HTF should be equal to that absorbed by the PCM (Q_{PCM}, kJ), LHTES SS_{HEX} and losses (Q_{Losses}, kJ), as in Equation 12.

$$Q_{HTF} = Q_{PCM} + Q_{SS_{HEX}} + Q_{Losses} \qquad \textit{Equation 12}$$

During the discharging of LHTES (i.e., cooling and thus freezing the PCM), the heat supplied by the PCM should be equal to that absorbed by the HTF, LHTES SS_{HEX} and losses, as in Equation 13.

$$Q_{PCM} = Q_{HTF} + Q_{SS_{HEX}} + Q_{Losses} \qquad \textit{Equation 13}$$

Theoretical maximum heat storage capacity of PCMs RT57HC and RT60HC in the LHTES

Between the full temperature range 35-79 °C considered in the data analysis the theoretical ES capacity for RT57HC and RT60HC each can be determined using their total masses in the LHTES as in Table 20, and the intrinsic thermal properties in Table 18 and Table 19, combining the latent heats of fusion and sensible heats. These are summarized in Table 22.

Table 22. Theoretical maximum heat storage capacity of PCMs RT57HC and RT60HC in LHTES

Theoretical storage capacity of	Heating (with melting)	Cooling (with freezing)
RT57HC (kJ)	20 502	-15 504
RT60HC (kJ)	14 620	-12 810

As seen in Table 22, the heating versus cooling total theoretical TES capacity (within 35-79 °C) difference is for RT60HC is ~12%, while that for RT60HC is ~24% different. These are rather significant, and more so for RT57HC. A key cause for these differences lie on the uncertianty of the calorimetric method employed (explained in section 6.1.2). While it is sufficiently accurate for determining the phase change enthalpy differences, it evidently requires more accurate supplements for determining the specific heat capacities of the respective (single) soild and liquid phases. Moreover, choosing the phase change boundaries have been not so straightforward particularly for melting (and or phase changes during heating), which is wider and thus somewhat gradual. These external (data processing) impacts on the accuracy are evdient also in the specific heat differences observed in e.g. Table 18 and Table 19, with e.g., too high specific heat capacities (c_p) particularly for solid1 and solid 2 in RT57HC. For RT60HC, this difference is smaller, yet still with higher c_p for solid state in heating than in cooling. Their uncertainties propagate over the wide temperature ranges where the PCM remains in a single

phase (storing sensible heat), and hence these differences also propagate, when calculating the total TES capacity of each PCM for the LHTES system volume.

These values however are considered in this study as the starting benchmark estimations of the expected of 'real' TES capacities calculated for each cycle.

Data analysis and final calculations

The final obtained cycled data for RT57HC and RT60HC respectively were post-processed to correct for temperature calibrations, and then their isothermal endpoints were filtered out (as that is not of interest for the final analysis). Thereafter, the parameter b calculation followed by full calculations as described in earlier sections were automated via using three respective Python calculation codes dedicated to RT57HC and RT60HC (given in Appendix B, sections B.1-B.3 with b calculation procedure explained in section B.4).

7.2. Results and Discussion – Bench-Scale PCM Testing

The main results concerning the bench-scale long-term cycling test of the 2 short-listed PCM candidates RT57HC and RT60HC intended for the HYSTORE solutions I and II are discussed concisely here.

Phase change temperature bounds and initial parameters in LHTES testing

When cycling the PCMs in the bench-scale LHTES system, it was observed that the bulk phase change temperatures were not exactly the same as those found with the material-intrinsic property analysis. Although respectively considering this apparent phase change temperature for each cycle and sensor, and then performing the TES calculations individually for that specific range for each cycle separately is the best, for analyzing data for 53 cycles, this is impractical. Therefore, it was decided to choose an initial cycle (cycle 3) respectively during cooling and heating for each PCM, to pick representative phase change temperature ranges. As there are 8 sensors producing these temperature data, to simplify, it was also decided to use 203, 205, 207 and 209 as representative points (and having similar temperature history trends to their respective counterparts 204, 206, 208 and 210). The mean of the identified phase change temperatures from the four sensors was then used as the overall phase change range for the given PCM and phase change (as RT57Hc has two phase changes) for heating and cooling respectively. These temperatures were then used to determine the T_{PC} to calculate *b* for Dirac function, and to apply the intrinsic property data for energy capacity estimation over the full number of cycles tested (27 for RT57HC and 50 for RT60HC). These temperatures, and the final b and final T_{PC} values used in the calculations are summarized in Table 23 for RT57HC, and Table 24 for RT60HC.

Table 23. Phase change temperature bounds and thus temperature ranges considered, and therein obtained b and T_{PC} values for RT57HC in LHTES (bulk PCM behavior)

Heating		(≈204) 203	(≈206) 205	(≈208) 207	(≈210) 209	Average	Unit
dT_S1	*Start: 35*					20.0	°C

S1 → S2	**PC1,start**	55.38	55.35	55.24	54.11	**55.0**	°C
	PC1,end	58.46	58.26	59.35	57.60	**58.4**	°C
dT_S2						3.6	°C
S2→ Liquid	**PC2,start**	61.05	61.55	63.37	62.17	**62.0**	°C
	PC2,end	61.88	62.4	64.27	63.89	**63.1**	°C
dT_Liquid	*End: 79*					15.9	°C
b for PC1	**b1**	0.845	0.798	1.128	0.958		
b for PC2	**b2**	0.225	0.233	0.247	0.472		
	T_{PC1}	56.92	56.805	57.295	55.855		
	T_{PC2}	61.47	61.98	63.82	63.03		
Cooling		**(≈204) 203**	**(≈206) 205**	**(≈208) 207**	**(≈210) 209**	**Average**	**Unit**
dT_Liquid	*Start: 79*					-21.7	°C
Liquid → S1	**PC1,start**	57.67	57.33	57.39	56.87	**57.3**	°C
	PC1,end	56.53	56.41	56.12	55.94	**56.3**	°C
dT_S2						-1.9	°C
S1→ S2	**PC2,start**	54.34	54.29	54.53	54.09	**54.3**	°C
	PC2,end	53.6	53.56	53.22	52.93	**53.3**	°C
dT_S1	*End: 35*					-18.3	°C
b for PC1	**b1**	0.285	0.253	0.321	0.255		
b for PC2	**b2**	0.203	0.2	0.359	0.316		
	T_{PC1}	57.1	56.87	56.755	56.40		
	T_{PC2}	53.97	53.93	53.88	53.51		

Here, dT: temperature difference; S1 and S2: the two solid phases in RT57HC; PC1 and PC2: phase change 1 and phase change 2, respectively

Table 24. Phase change temperature bounds and thus temperature ranges considered, and therein obtained b and T_{PC} values for RT60HC in LHTES (bulk PCM behavior)

Heating		**(≈204) 203**	**(≈206) 205**	**(≈208) 207**	**(≈210) 209**	**Average**	**Unit**
dT_Solid	*Start: 35*					21.1	°C
Solid → Liquid	**PC,start**	56.79	56.69	55.86	55.02	**56.1**	°C
	PC,end	62.24	62.22	63.17	61.3	**62.2**	°C
dT_Liquid	*End: 79*					16.8	°C
	b	1.496	1.518	2.007	1.724		
	T_{PC}	59.52	59.46	59.52	58.16		
Cooling		**(≈204) 203**	**(≈206) 205**	**(≈208) 207**	**(≈210) 209**	**Average**	**Unit**
dT_Liquid	*Start: 79*					-18.1	°C
Liquid → Solid	**PC,start**	60.85	60.92	61.3	60.71	**60.9**	°C
	PC,end	58.92	59.26	58.94	58.4	**58.9**	°C
dT_Solid	*End: 35*					-23.9	°C
	b	0.529	0.456	0.648	0.634		
	T_{PC}	61.82	61.75	62.48	61.87		

Here, dT: temperature difference; S1 and S2: the two solid phases in RT57HC; PC: phase change

Examples of the temperature choices summarized in Table 23 and Table 24, from the heating and cooling cycles are shown respectively in Figure 44 and Figure 45 for RT57HC and in Figure 46 and Figure 47 for RT60HC.

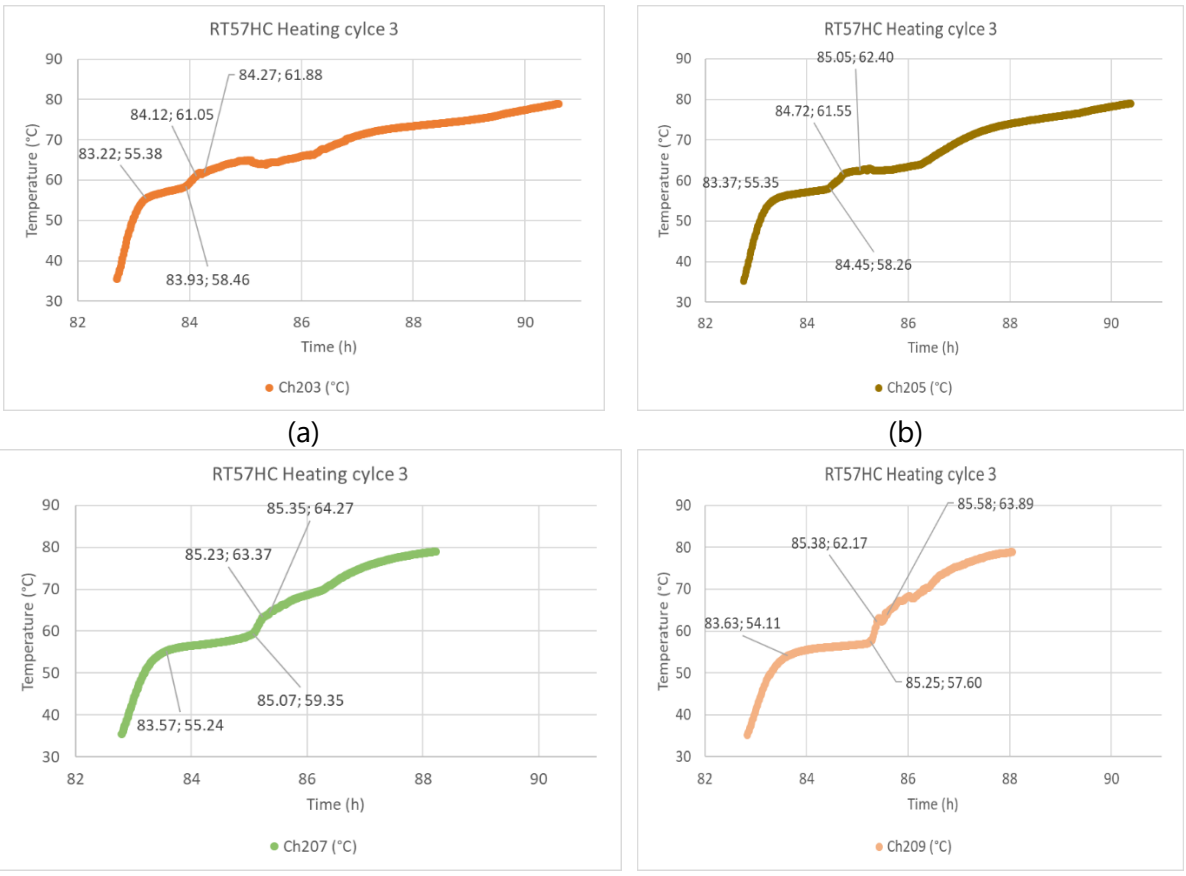

Figure 44. RT57HC heating cycle 3, temperature bound choices in temperature sensors 203, 205, 207 and 209 from LHTES, in (a)-(d)

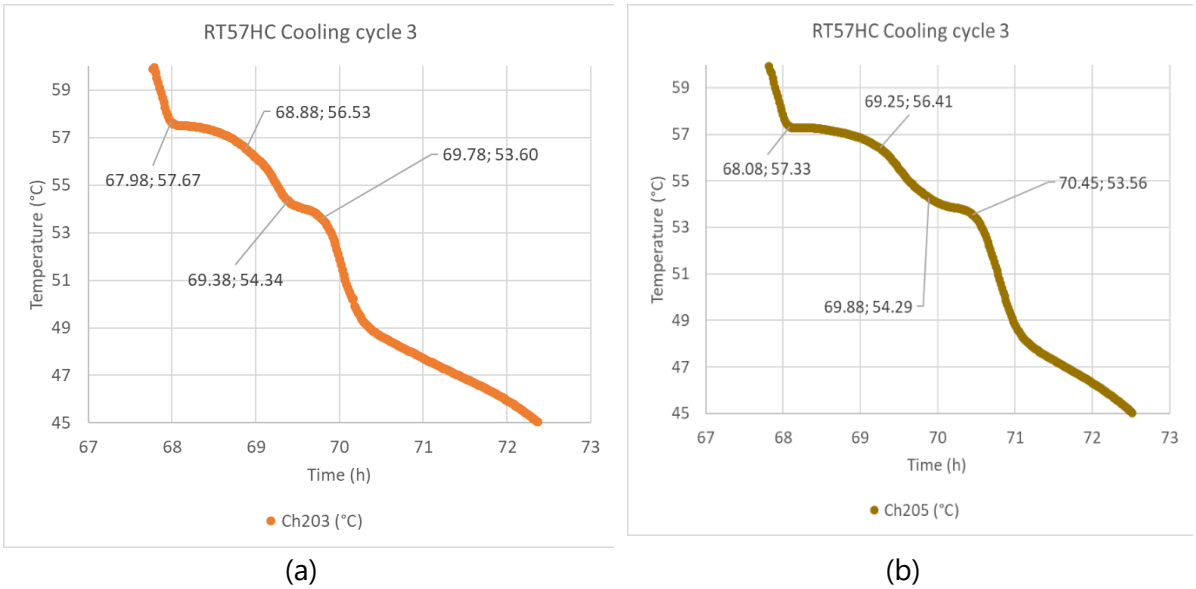

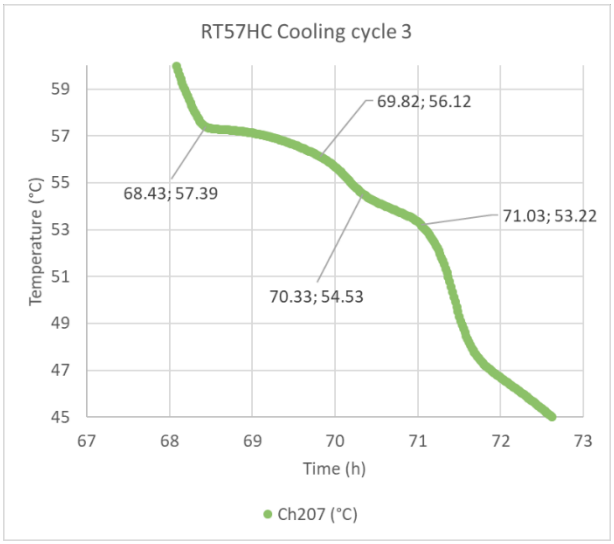

(c)

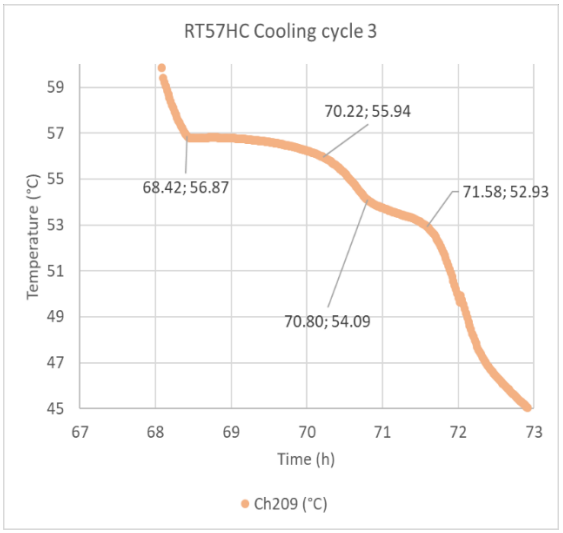

(d)

Figure 45. RT57HC cooling cycle 3, temperature bound choices in temperature sensors 203, 205, 207 and 209 from LHTES, in (a)-(d)

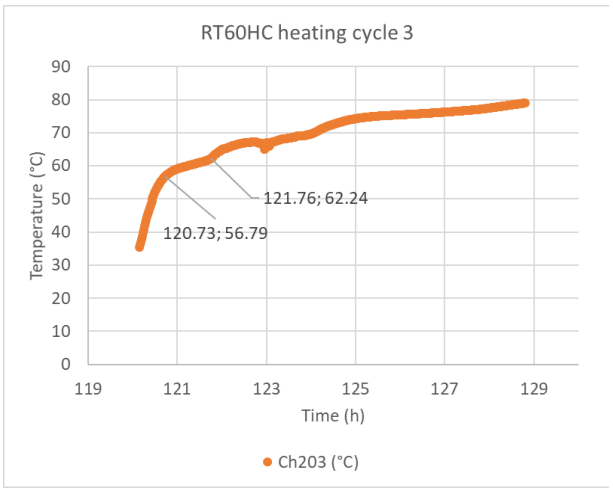

(a)

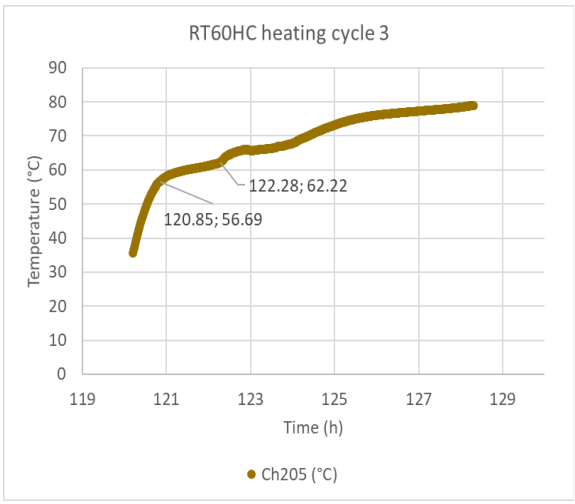

(b)

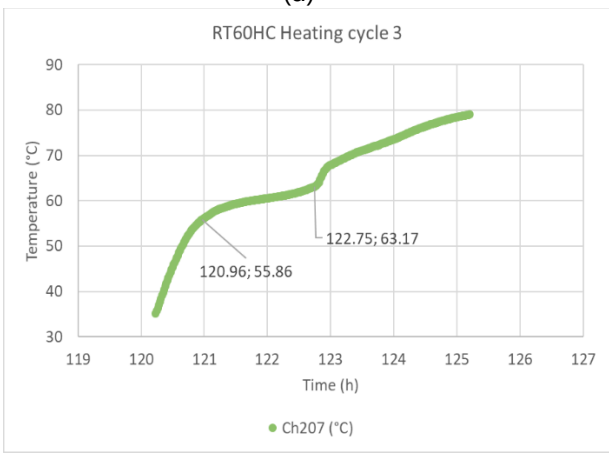

(c)

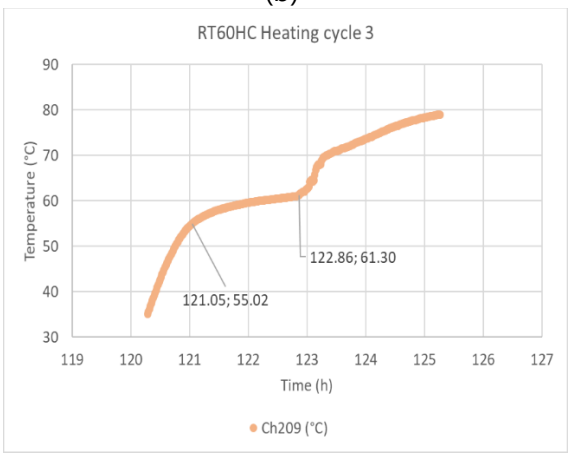

(d)

Figure 46. RT60HC heating cycle 3, temperature bound choices in temperature sensors 203, 205, 207 and 209 from LHTES, in (a)-(d)

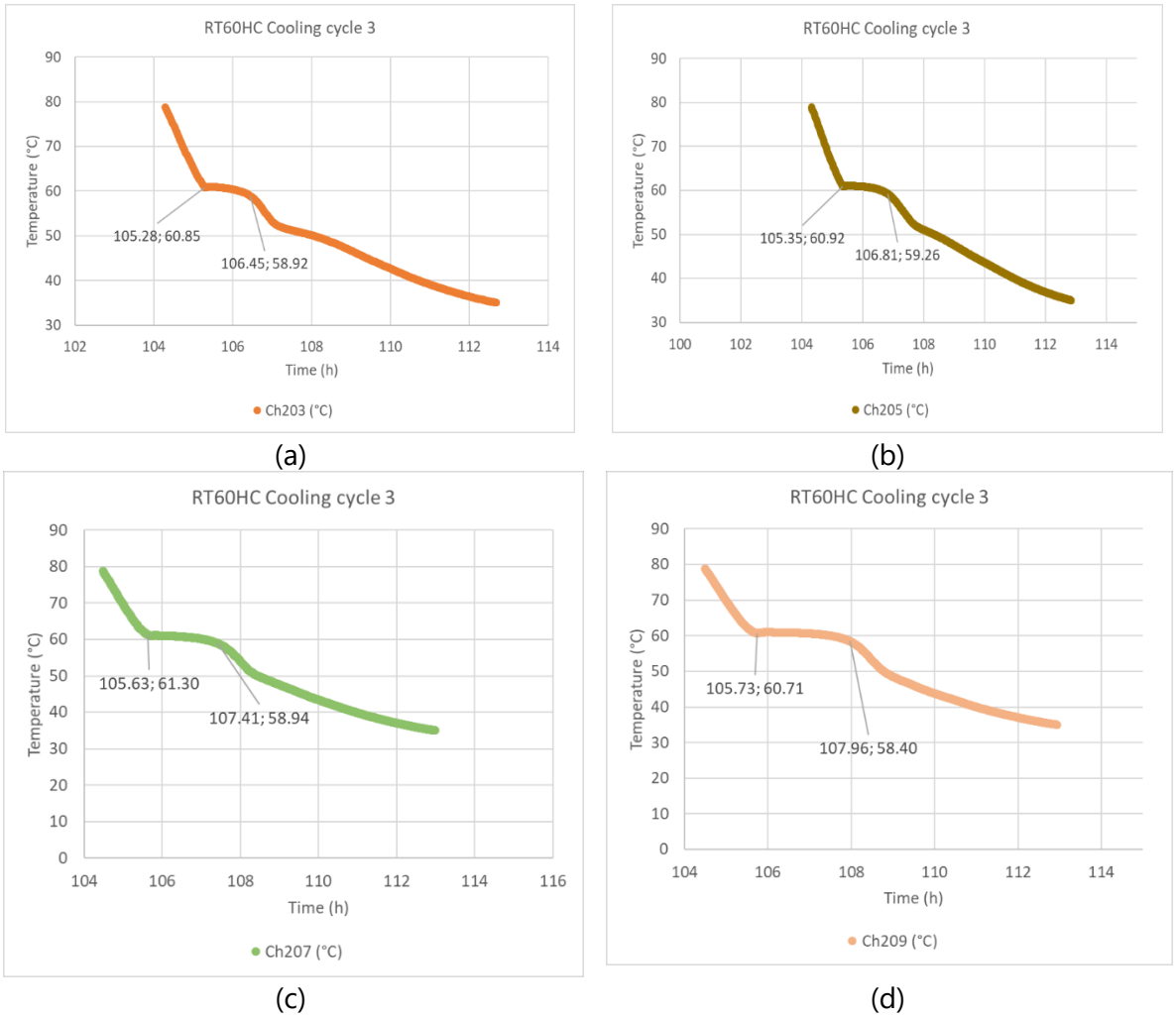

Figure 47. RT60HC cooling cycle 3, temperature bound choices in temperature sensors 203, 205, 207 and 209 from LHTES, in (a)-(d)

As seen in Figure 44 and in Figure 46, both PCMs' temperature profiles have some artifact effects during heating, at temperatures around and within 65-70 °C, on the 203 and 205, i.e., the sensors placed at the upper half of the LHTES. This is reasoned as most possibly due to bulk chunks of PCM that was attached to these upper-level sensors fall down when they start melting, towards the already molten PCM at the lower-parts of the LHTES. This is plausible as the HTF inlet is at the bottom half of the LHTES cylinder (with 201) and the outlet is from the upper half (with 202). Thus it is inevitable that there is a temperature gradient from the bottom to top of the LHTES as well as from left to right, causing temperature inhomogeneity and therefore differences in the phase change rate at local points within the TES unit.

Cycling test results highlights

The complete cycling temperature-history respectively of RT57HC (27 cycles) and RT60HC (53 cycles) for heating (i.e., melting or charging) and cooling (i.e., freezing or discharging) are shown in Figure 48, Figure 49 and Figure 50 (RT57HC) and Figure 51, Figure 52 and Figure 53 (RT60HC), taking sensors 203, 205 and 207 as examples. As observable, both PCMs show quite consistent phase change behavior throughout these extensive cycling.

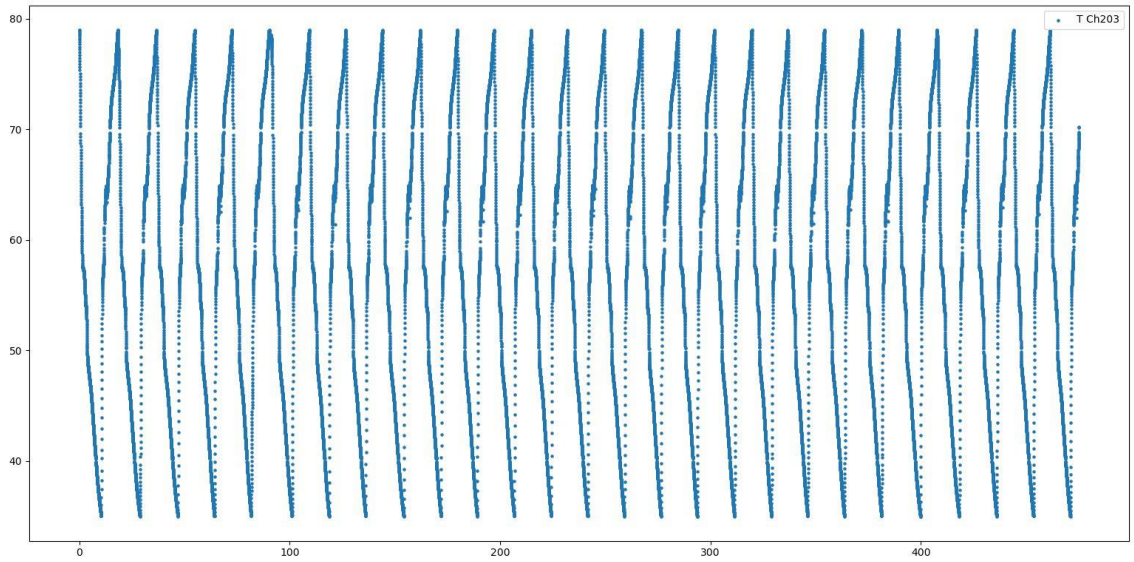

Figure 48. RT57HC cycling behavior in the LHTES for 27 cycles, captured with sensor 203

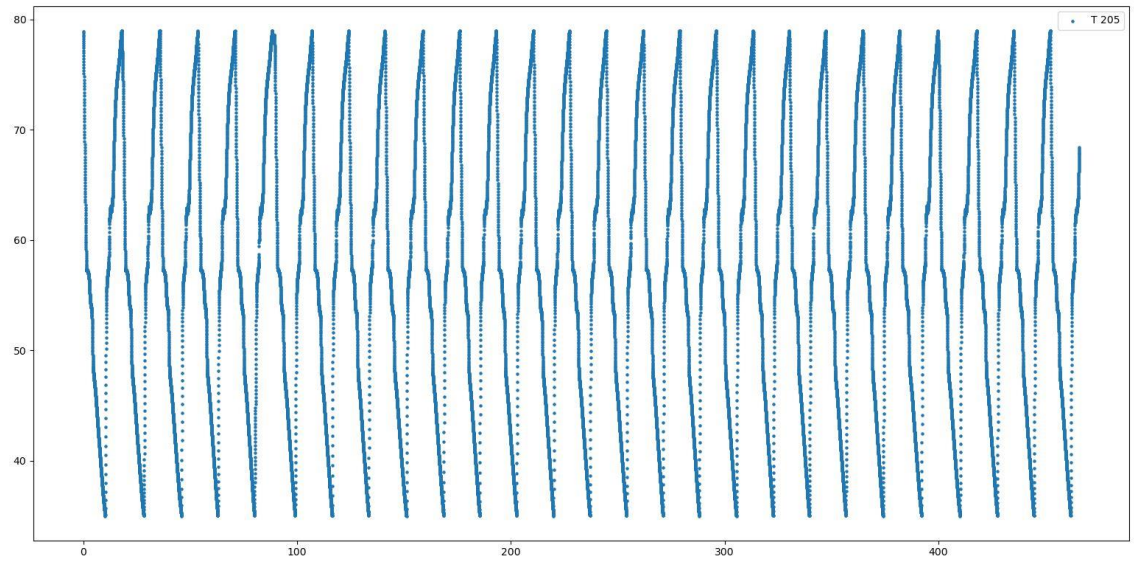

Figure 49. RT57HC cycling behavior in the LHTES for 27 cycles, captured with sensor 205

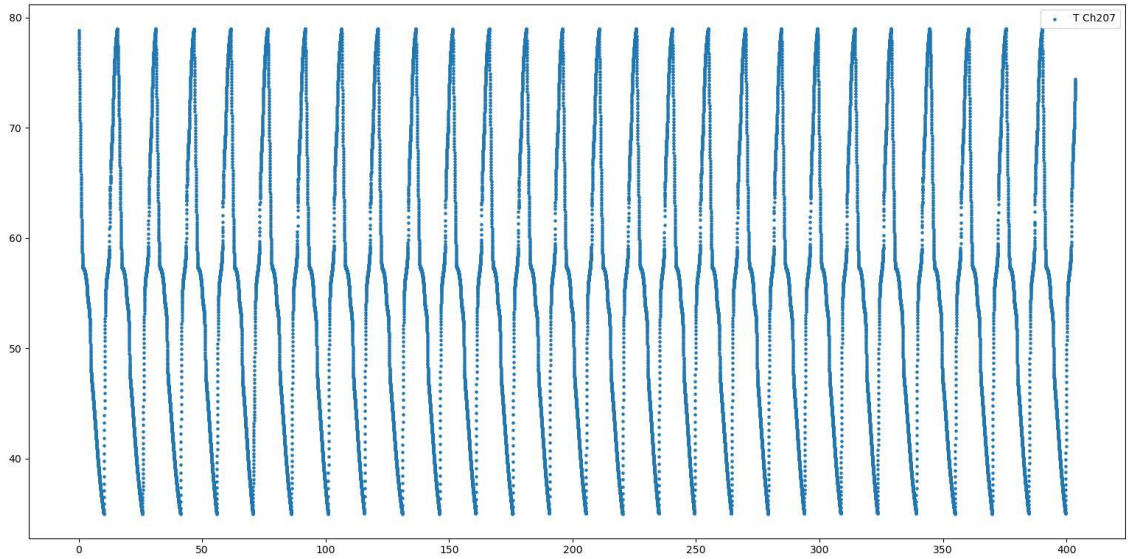

Figure 50. RT57HC cycling behavior in the LHTES for 27 cycles, captured with sensor 207

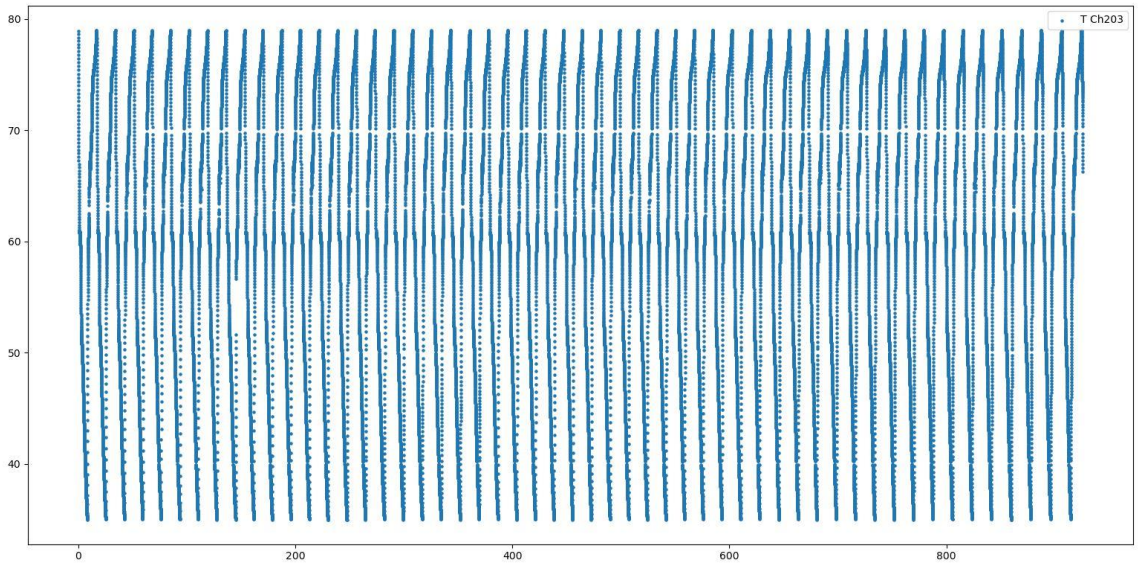

Figure 51. RT60HC cycling behavior in the LHTES for 53 cycles, captured with sensor 203

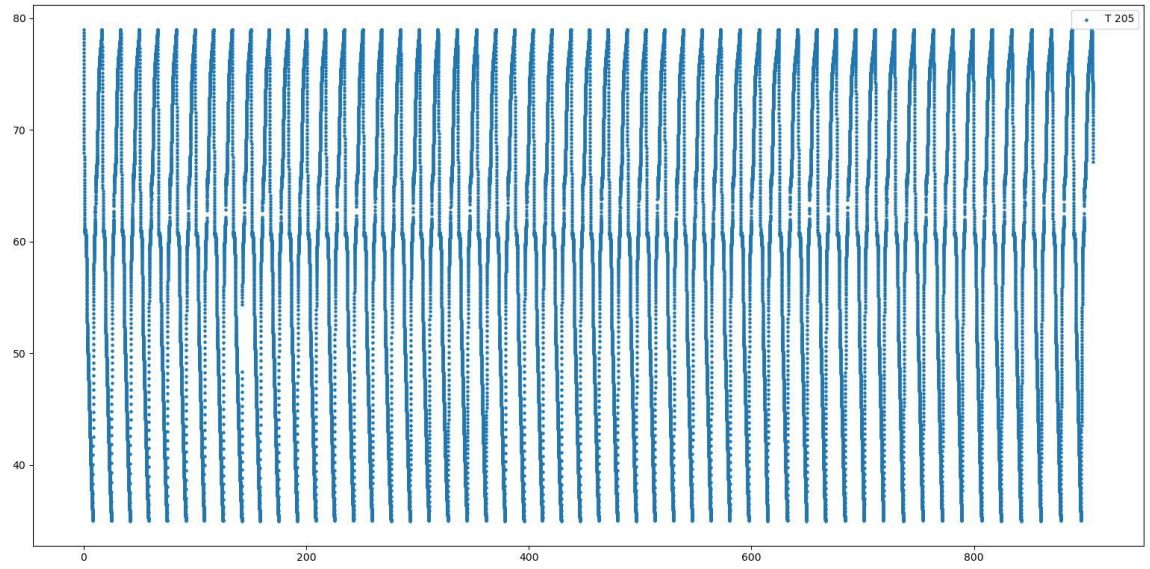

Figure 52. RT60HC cycling behavior in the LHTES for 53 cycles, captured with sensor 205

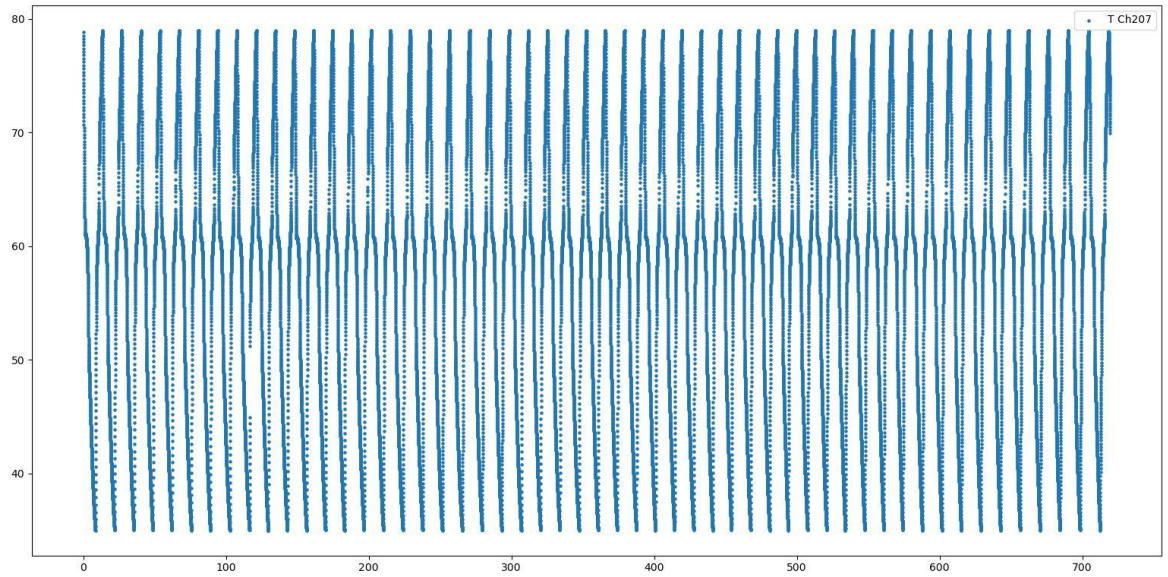

Figure 53. RT60HC cycling behavior in the LHTES for 53 cycles, captured with sensor 207

Their final LHTES capacities and their comparison to the heat from/to HTF and the SSHEX and thus the losses are summarized in Table 25 and Table 26 for RT57HC and in Table 27 and Table 28 for RT60HC.

Table 25. RT57HC LHTES capacity, energy delivered by HTF and heat losses for 27 heating cycles

No. Cycle	TES capacity from PCM [kJ]	%difference of each cycle Vs. average	HTF [kJ]	%difference of each cycle Vs. average	Heat stored in the Stainless Steel (kJ)	Heat losses (kJ)	Real % of energy loss
Cycle 1	19135	0.51%	-15516	0.1%	3300	319	-2.1%

Cycle 2	19289	0.30%	-15015	2.7%	3300	974	-6.5%
Cycle 3	19215	0.09%	-15695	0.8%	3300	220	-1.4%
Cycle 4	19321	0.46%	-15884	1.8%	3300	137	-0.9%
Cycle 5	19296	0.33%	-15941	2.1%	3300	54	-0.3%
Cycle 6	19284	0.27%	-15679	0.8%	3300	306	-1.9%
Cycle 7	19219	0.07%	-15757	1.2%	3300	163	-1.0%
Cycle 8	19261	0.15%	-15392	0.7%	3300	569	-3.7%
Cycle 9	19197	0.18%	-15444	0.5%	3300	454	-2.9%
Cycle 10	19212	0.11%	-15428	0.6%	3300	484	-3.1%
Cycle 11	19202	0.16%	-15407	0.7%	3300	495	-3.2%
Cycle 12	19268	0.19%	-15778	1.3%	3300	190	-1.2%
Cycle 13	19199	0.17%	-15364	0.9%	3300	535	-3.5%
Cycle 14	19272	0.21%	-15041	2.6%	3300	931	-6.2%
Cycle 15	19297	0.34%	-15731	1.0%	3300	266	-1.7%
Cycle 16	19223	0.05%	-15664	0.7%	3300	259	-1.7%
Cycle 17	19249	0.09%	-15659	0.7%	3300	290	-1.9%
Cycle 18	19276	0.22%	-15748	1.1%	3300	228	-1.4%
Cycle 19	19286	0.28%	-15341	1.0%	3300	645	-4.2%
Cycle 20	19314	0.42%	-15136	2.1%	3300	878	-5.8%
Cycle 21	19281	0.25%	-15735	1.0%	3300	246	-1.6%
Cycle 22	19290	0.30%	-15613	0.4%	3300	377	-2.4%
Cycle 23	19233	0.00%	-15523	0.1%	3300	410	-2.6%
Cycle 24	19279	0.24%	-15510	0.1%	3300	469	-3.0%
Cycle 25	19301	0.35%	-15631	0.5%	3300	370	-2.4%
Cycle 26	19298	0.34%	-15230	1.6%	3300	768	-5.0%
Cycle 27	18574	3.42%	-15551	0.1%	3300	-277	1.8%
Average [kJ]	**19232**		**-15534**		**3300**	398	-2.6%
Average [kWh]	**5.2**						

Table 26. RT57HC LHTES capacity, energy delivered by HTF and heat losses for 27 cooling cycles

No. Cycle	TES capacity from PCM [kJ]	%difference of each cycle Vs. average	HTF [kJ]	%difference of each cycle Vs. average	Heat stored in the Stainless Steel (kJ)	Heat losses (kJ)	Real % of energy loss
Cycle 1	-15767	0.49%	11630	0.80%	3300	-837	5.3%
Cycle 2	-15881	0.11%	11880	2.10%	3300	-702	4.4%
Cycle 3	-15876	0.08%	11545	0.35%	3300	-1032	6.5%
Cycle 4	-15838	0.12%	11697	1.15%	3300	-841	5.3%
Cycle 5	-15865	0.02%	11391	0.44%	3300	-1174	7.4%
Cycle 6	-15890	0.15%	11202	1.43%	3300	-1388	8.7%

Cycle 7	-15855	0.03%	11476	0.00%	3300	-1079	6.8%
Cycle 8	-15867	0.03%	11413	0.33%	3300	-1154	7.3%
Cycle 9	-15874	0.07%	11502	0.13%	3300	-1072	6.8%
Cycle 10	-15851	0.05%	11574	0.51%	3300	-977	6.2%
Cycle 11	-15857	0.02%	11437	0.21%	3300	-1120	7.1%
Cycle 12	-15865	0.02%	11379	0.51%	3300	-1186	7.5%
Cycle 13	-15857	0.02%	11467	0.05%	3300	-1090	6.9%
Cycle 14	-15868	0.04%	11426	0.26%	3300	-1142	7.2%
Cycle 15	-15861	0.00%	11357	0.62%	3300	-1204	7.6%
Cycle 16	-15857	0.02%	11325	0.78%	3300	-1232	7.8%
Cycle 17	-15865	0.02%	11248	1.19%	3300	-1317	8.3%
Cycle 18	-15870	0.05%	11289	0.97%	3300	-1282	8.1%
Cycle 19	-15862	0.01%	11316	0.83%	3300	-1246	7.9%
Cycle 20	-15865	0.02%	11278	1.03%	3300	-1287	8.1%
Cycle 21	-15864	0.02%	11265	1.10%	3300	-1300	8.2%
Cycle 22	-15862	0.00%	11229	1.29%	3300	-1333	8.4%
Cycle 23	-15878	0.09%	11587	0.57%	3300	-991	6.2%
Cycle 24	-15882	0.11%	11871	2.05%	3300	-711	4.5%
Cycle 25	-15859	0.01%	11739	1.36%	3300	-820	5.2%
Cycle 26	-15853	0.04%	11671	1.01%	3300	-882	5.6%
Cycle 27	-15852	0.04%	11669	1.00%	3300	-883	5.6%
Average [kJ]	**-15861**		**11476**		3300	-1085	6.8%
Average [kWh]	**4.4**						

Table 27. RT60HC LHTES capacity, energy delivered by HTF and heat losses for 53 heating cycles

No. Cycle	TES capacity from PCM [kJ]	%difference of each cycle Vs. average	HTF [kJ]	%difference of each cycle Vs. average	Heat losses (including heat stored in tank)	Heat stored in the Stainless Steel (kJ)	% heat loss
Cycle 1	14982	1.77%	-14288	3.40%	3994	3300	-5%
Cycle 2	15282	0.20%	-14743	0.32%	3839	3300	-4%
Cycle 3	15203	0.31%	-14612	1.21%	3891	3300	-4%
Cycle 4	15253	0.01%	-14298	3.33%	4255	3300	-7%
Cycle 5	15250	0.00%	-14511	1.89%	4039	3300	-5%
Cycle 6	15233	0.12%	-14528	1.78%	4005	3300	-5%
Cycle 7	15248	0.02%	-14521	1.82%	4026	3300	-5%
Cycle 8	15242	0.06%	-14278	3.46%	4264	3300	-7%
Cycle 9	15368	0.76%	-13266	10.31%	5402	3300	-16%
Cycle 10	15241	0.07%	-14312	3.24%	4229	3300	-6%

Cycle 11	15256	0.04%	-14546	1.65%	4010	3300	-5%
Cycle 12	15255	0.03%	-14553	1.61%	4003	3300	-5%
Cycle 13	15262	0.08%	-14676	0.77%	3886	3300	-4%
Cycle 14	15254	0.02%	-14795	0.03%	3759	3300	-3%
Cycle 15	15243	0.05%	-14542	1.68%	4001	3300	-5%
Cycle 16	15250	0.01%	-14348	3.00%	4202	3300	-6%
Cycle 17	15261	0.07%	-14424	2.48%	4138	3300	-6%
Cycle 18	15238	0.09%	-14347	3.00%	4190	3300	-6%
Cycle 19	15253	0.01%	-14076	4.84%	4477	3300	-8%
Cycle 20	15258	0.04%	-14187	4.09%	4371	3300	-8%
Cycle 21	15265	0.09%	-14448	2.31%	4117	3300	-6%
Cycle 22	15254	0.02%	-14542	1.68%	4011	3300	-5%
Cycle 23	15225	0.17%	-14680	0.75%	3845	3300	-4%
Cycle 24	15236	0.10%	-14446	2.33%	4089	3300	-5%
Cycle 25	15260	0.06%	-14455	2.27%	4105	3300	-6%
Cycle 26	15289	0.25%	-14704	0.59%	3885	3300	-4%
Cycle 27	15228	0.15%	-14793	0.01%	3735	3300	-3%
Cycle 28	15256	0.03%	-14567	1.51%	3989	3300	-5%
Cycle 29	15265	0.09%	-14655	0.92%	3910	3300	-4%
Cycle 30	15266	0.10%	-14758	0.22%	3808	3300	-3%
Cycle 31	15257	0.04%	-14618	1.17%	3939	3300	-4%
Cycle 32	15273	0.14%	-14678	0.76%	3895	3300	-4%
Cycle 33	15270	0.12%	-14872	0.55%	3698	3300	-3%
Cycle 34	15227	0.15%	-14842	0.34%	3686	3300	-3%
Cycle 35	15247	0.02%	-15038	1.67%	3509	3300	-1%
Cycle 36	15266	0.10%	-15372	3.93%	3194	3300	1%
Cycle 37	15247	0.03%	-15379	3.98%	3168	3300	1%
Cycle 38	15250	0.01%	-15368	3.90%	3182	3300	1%
Cycle 39	15235	0.11%	-15025	1.59%	3509	3300	-1%
Cycle 40	15275	0.15%	-15162	2.51%	3413	3300	-1%
Cycle 41	15255	0.03%	-15124	2.25%	3431	3300	-1%
Cycle 42	15234	0.11%	-15431	4.33%	3102	3300	1%
Cycle 43	15255	0.03%	-15380	3.98%	3175	3300	1%
Cycle 44	15270	0.13%	-15260	3.17%	3310	3300	0%
Cycle 45	15249	0.02%	-15198	2.75%	3351	3300	0%
Cycle 46	15271	0.13%	-15190	2.70%	3381	3300	-1%
Cycle 47	15274	0.15%	-15320	3.58%	3254	3300	0%
Cycle 48	15253	0.01%	-15110	2.16%	3443	3300	-1%
Cycle 49	15256	0.03%	-15137	2.34%	3419	3300	-1%
Cycle 50	15283	0.21%	-15279	3.30%	3304	3300	0%
Cycle 51	15261	0.07%	-15340	3.72%	3221	3300	1%
Cycle 52	15256	0.04%	-15642	5.75%	2915	3300	2%

Cycle 53	15265	0.09%	-15748	6.47%	2817	3300	3%
Average [kJ]	**15251**		**-14791**		**460**		**-3%**
Average [kWh]	**4.24**						

Table 28. RT60HC LHTES capacity, energy delivered by HTF and heat losses for 53 cooling cycles

No. Cycle	TES capacity from PCM [kJ]	%difference of each cycle Vs. average	HTF [kJ]	%difference of each cycle Vs. average	Heat stored in the Stainless Steel (kJ)	Heat losses (kJ)	% heat loss
Cycle 1	-13201	2.28%	11524	3.50%	3300	1623	-12%
Cycle 2	-13511	0.02%	11621	4.21%	3300	1410	-10%
Cycle 3	-13498	0.08%	11766	5.29%	3300	1568	-12%
Cycle 4	-13468	0.30%	11576	3.88%	3300	1408	-10%
Cycle 5	-13547	0.29%	11130	0.58%	3300	882	-7%
Cycle 6	-13511	0.02%	11234	1.35%	3300	1023	-8%
Cycle 7	-13479	0.22%	11127	0.55%	3300	948	-7%
Cycle 8	-13545	0.27%	11196	1.07%	3300	951	-7%
Cycle 9	-13519	0.07%	11275	1.65%	3300	1057	-8%
Cycle 10	-13488	0.16%	11156	0.77%	3300	968	-7%
Cycle 11	-13523	0.10%	11122	0.52%	3300	899	-7%
Cycle 12	-13495	0.10%	11120	0.50%	3300	925	-7%
Cycle 13	-13490	0.13%	11015	0.28%	3300	824	-6%
Cycle 14	-13514	0.04%	10950	0.75%	3300	737	-5%
Cycle 15	-13532	0.17%	11147	0.70%	3300	915	-7%
Cycle 16	-13506	0.02%	11055	0.02%	3300	849	-6%
Cycle 17	-13529	0.15%	11030	0.16%	3300	801	-6%
Cycle 18	-13499	0.07%	11052	0.00%	3300	853	-6%
Cycle 19	-13525	0.12%	11051	0.00%	3300	827	-6%
Cycle 20	-13528	0.14%	11003	0.36%	3300	775	-6%
Cycle 21	-13487	0.16%	11020	0.24%	3300	832	-6%
Cycle 22	-13497	0.09%	10929	0.91%	3300	732	-5%
Cycle 23	-13512	0.03%	11287	1.74%	3300	1075	-8%
Cycle 24	-13505	0.03%	11308	1.89%	3300	1103	-8%
Cycle 25	-13509	0.00%	11187	1.00%	3300	978	-7%
Cycle 26	-13515	0.05%	11357	2.25%	3300	1142	-8%
Cycle 27	-13478	0.23%	11333	2.08%	3300	1155	-9%
Cycle 28	-13514	0.04%	11288	1.75%	3300	1074	-8%
Cycle 29	-13511	0.02%	11292	1.78%	3300	1081	-8%
Cycle 30	-13499	0.07%	11272	1.63%	3300	1073	-8%
Cycle 31	-13505	0.03%	11280	1.69%	3300	1076	-8%

Cycle 32	-13512	0.03%	11211	1.18%	3300	999	-7%
Cycle 33	-13489	0.15%	11148	0.71%	3300	960	-7%
Cycle 34	-13500	0.06%	11045	0.05%	3300	844	-6%
Cycle 35	-13516	0.06%	10997	0.41%	3300	781	-6%
Cycle 36	-13495	0.10%	11011	0.30%	3300	816	-6%
Cycle 37	-13495	0.10%	10873	1.33%	3300	678	-5%
Cycle 38	-13534	0.19%	10833	1.62%	3300	599	-4%
Cycle 39	-13506	0.02%	10910	1.05%	3300	704	-5%
Cycle 40	-13512	0.03%	10899	1.13%	3300	687	-5%
Cycle 41	-13518	0.07%	10813	1.77%	3300	595	-4%
Cycle 42	-13502	0.05%	10841	1.57%	3300	638	-5%
Cycle 43	-13512	0.03%	10727	2.41%	3300	515	-4%
Cycle 44	-13523	0.11%	10763	2.14%	3300	539	-4%
Cycle 45	-13508	0.01%	10775	2.05%	3300	567	-4%
Cycle 46	-13510	0.01%	10692	2.66%	3300	483	-4%
Cycle 47	-13510	0.01%	10697	2.63%	3300	486	-4%
Cycle 48	-13512	0.03%	10677	2.77%	3300	465	-3%
Cycle 49	-13515	0.05%	10573	3.54%	3300	358	-3%
Cycle 50	-13508	0.01%	10555	3.68%	3300	347	-3%
Cycle 51	-13510	0.01%	10721	2.45%	3300	511	-4%
Cycle 52	-13512	0.03%	10713	2.51%	3300	501	-4%
Cycle 53	-13509	0.00%	10612	3.26%	3300	403	-3%
Average [kJ]	**-13509**		**11052**		**3300**	**543**	**-4%**
Average [kWh]	**-3.8**						

As can be further verified from Table 25-Table 28, the TES capacities are quite consistent (and quite reasonable within the uncertainties at this bulk level testing) for all the cycles. Their average TES capacities (calculated considering the PCM) for these 'real tests' are summarized and compared against the corresponding theoretical maximum values (from Table 22) in Table 29.

As seen, the difference of PCM-TES average capacities between heating and cooling in the real test is 18% for RT57HC and 11% for RT60HC, while is 24% for RT57HC and 12% for RT60HC in theoretical estimates. These are thus rather comparable, whilst RT57HC has a more prominent dissimilarity (between 18% and 24%). The differences here between the theoretical versus real test values are mainly due to the differences in the temperature ranges applied for the different phases in the theoretical extimation (using intrinsic property data from RUBI, in Table 18 and Table 19) versus real LHTES testing (applying 'apparent' phase change temepratures on the temperature-history of the PCM in the LHTES, as in Table 23 and Table 24). Moreover, in the real LHTES, as certain sensors had rather different temperature-histories, the average temperature profile was used for practical reasons, which might add to uncertainty here.

Nevertheless, both PCMs displayed quite consistent TES capacities between their different cycles. On the other hand, when comparing the theoretical versus real test average PCM_TES capacities respectively for heating (6% and 4% differences) and cooling (2% and 5% differences) for RT57HC and RT60HC, these are still quite comparable.

Table 29. RT57HC and RT60HC PCM-TES capacities average summary: 'Theoretical' versus 'Real test' and heating versus cooling (in theoretical and real test data respectively) comparison

	kJ	kJ	kJ	kJ	Theoretical' versus 'Real test' difference (%)		Difference in 'Theoretical' values (%)	Difference in 'Real test' values (%)
	Real test		Theoretical maximum		in heating	in cooling	Heating versus cooling	
	heating	cooling	heating	cooling				
RT57HC	19232	15861	20502	15504	6.2%	-2.3%	24%	18%
RT60HC	15251	13509	14620	12810	-4.3%	-5.5%	12%	11%

The average power estimated on each respective temperature sensor during heating and cooling respectively are also shown in Figure 54 and Figure 55for RT57HC and in Figure 56 and Figure 57 for RT60HC. While there are differences in the power evolution from one cycle to another, it is evident that the overall power evolution trend remains consistent for the temperature sensors. Meaning, the sensors and thus the local charging/discharging power around that show consistent behavior mainly only influenced by the global heat transfer variations in the LHTES as a whole.

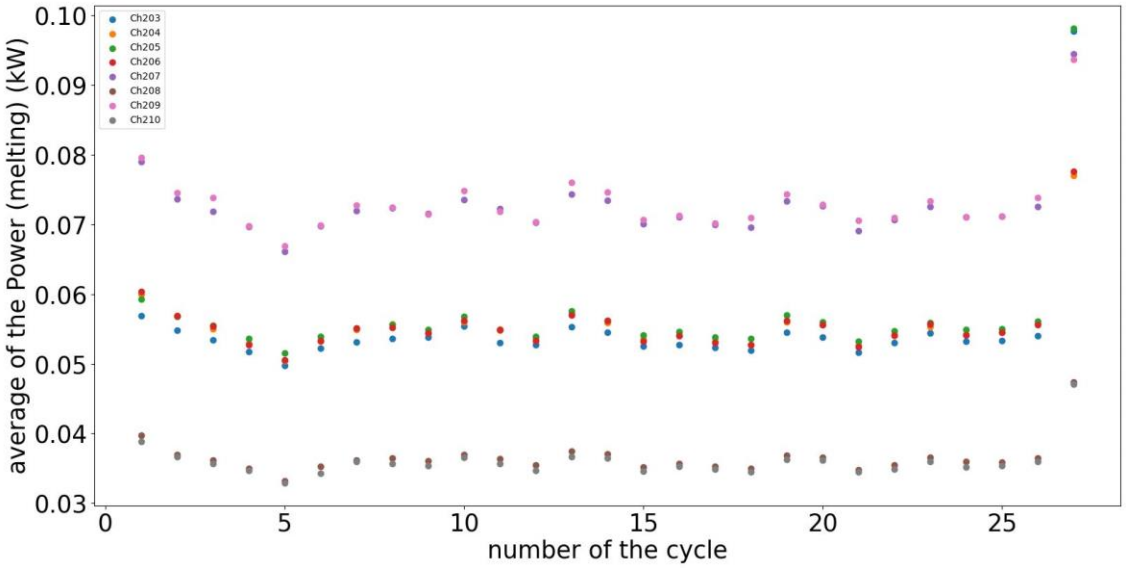

Figure 54. Average power (kW) per temperature sensor (channel) for RT57HC during heating (i.e., charging → melting)

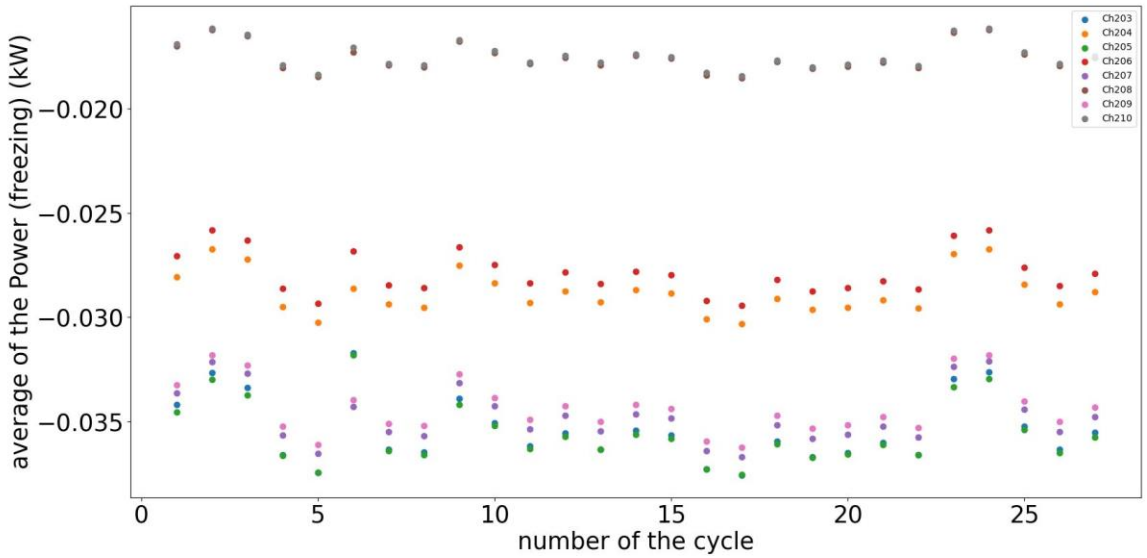

Figure 55. Average power (kW) per temperature sensor (channel) for RT57HC during cooling (i.e., discharging → freezing)

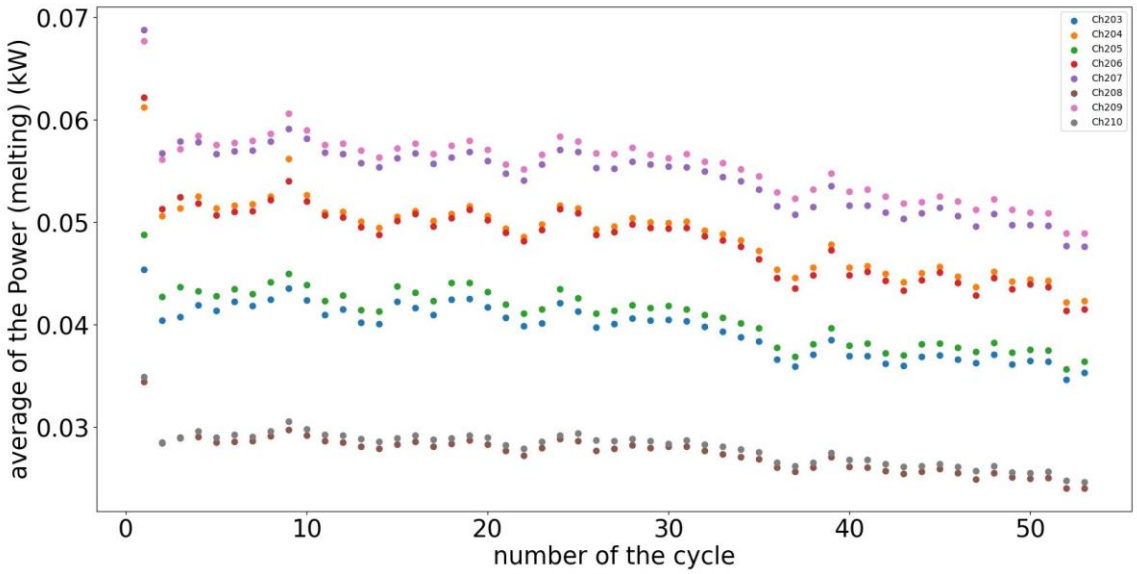

Figure 56. Average power (kW) per temperature sensor (channel) for RT60HC during heating (i.e., charging → melting)

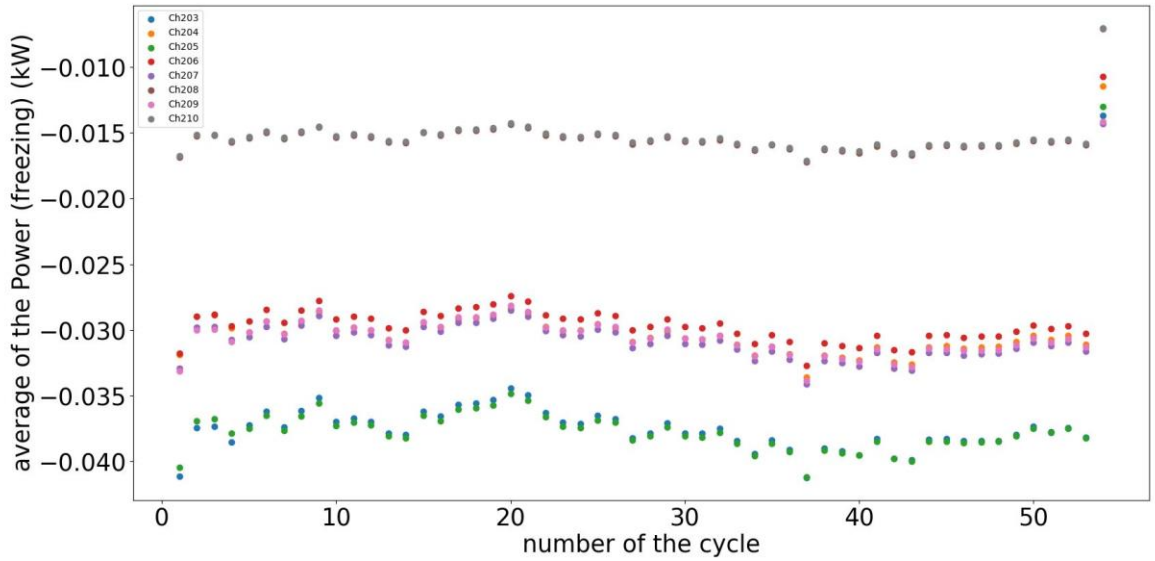

Figure 57. Average power (kW) per temperature sensor (channel) for RT60HC during cooling (i.e., discharging → freezing)

Supercooling, hysteresis and cycling stability

As seen in the single-cycle close-ups in Figure 44 - Figure 47 as well as the full cycling behavior in Figure 48 -Figure 53 it can be concluded that neither RT57HC nor RT60HC show any noticeable supercooling.

Hysteresis in PCMs is the difference between the melting and freezing temperatures observed. However, when this is defined in reality, particularly for PCMs with more than one phase change, application of this definition could vary based on the purpose of the application of the hysteresis data. In this investigation, the main purpose is to ensure that the entire phase change range during both heating (i.e., charging) and cooling (i.e., discharging) cycles are well within the full application temperature range. With that in focus, the attributes of hysteresis are defined per several aspects in this investigation such as the respective temperature ranges:

- For complete melting
- For complete freezing
- The start of the melting to the end of freezing
- The end of melting to the start of freezing
- Maximum operating range

As RT57HC displays two phase changes, end of melting or freezing means that both these phase changes are completed. These attributes in the bulk LHTES level vary slightly in the measurement of each temperature sensor due to temperature inhomogeneity in the TES unit. Nonetheless, using the same 3rd cycle respectively for heating and cooling for each PCM (c.f. Table 23, Table 24, Figure 44, Figure 45, Figure 46 and Figure 47), their hysteresis attributes can be summarized as in Table 30 using the average ranges from sensors 203, 205, 207 and 209 as a reasonable representative. As seen, the widest temperature range is for complete phase change in RT57HC and RT60HC is respectively 55- 63 °C (i.e., an 8 °C gap) and 56-62 °C (i.e., a 6 °C gap), which appears to occur during melting. Hence this also becomes the key

hysteresis characteristic that the TES design should fulfill, while it is still rather narrow considering the application temperature ranges for HYSTORE Solutions I and III. This hysteresis is still rather considerable for HYSTORE solution I in particular, for having a quite narrow (5 K) temperature range required per heat pump characteristics.

Table 30. Average hysteresis characteristics of RT57HC and RT60HC in bulk in LHTES cycling

Hysteresis characteristic	**RT57HC (in °C)**		**RT60HC (in °C)**	
Complete melting range	8	55.0-63.1	6	56.1-62.2
Complete freezing range	4	57.3-53.3	2	60.9-58.9
Start of melting to end of freezing	2	55.0-53.3	5	56.1-58.9
End of melting to start of freezing	6	63.1-57.3	1	62.2-60.9
Maximum operating range	8	55.0-63.1	6	56.1-62.2

Based on all the observations, it appears that both RT57HC and RT60HC have quite satisfactory cycling stability for a considerable number of cycles (27 and 53 respectively). Upon the completion of the 27th cycle, RT57HC also appeared quite similar to the initial state by color, i.e., transparent and colorless, as shown in Figure 58. While RT60HC main cycling tests are completed, the LHTES still contains the PCM, which will be cycled a few times every now and then in the coming year to have further verification of its stability. Hence, no final after long-term cycling samples are available yet, to check its final color.

(a) (b)

Figure 58. Appearance of RT57HC which remained the same (a) prior to any thermal cycling and (b) also after all the 27 cycling in the LHTES

Impacts on LHTES Internal pressure, mechanical strength and integrity

The influence of volume shrinkage and expansion of the two PCMs RT57HC and RT60HC upon cooling and heating on LHTES were not intentionally measured. It was indeed observed that RT57HC and RT60HC had higher volumes in liquid state (i.e., 49.4 l and 47.4 l respectively) than in solid state (i.e., 44.9 l and 44.0 l respectively). However, the LHTES was initially filled while maintaining it at 85 °C and also the PCMs at ~85 °C in molten state, the maximum volumes of both the PCMs and LHTES unit were matched at the upper limit of operational temperature (in the LHTES). Therefore, any possible additional stresses on the system due to volume expansion was minimized. On the other hand, when the solid contracted, no discernible impacts were identified to the LHTES internal pressure or mechanical integrity.

Also during the LHTES operation with the two PCMs, even despite the container system being completely closed during the thermal cycling, no leakage or structural integrity issues were observed. When the PCM inlet valve was opened during a heating cycle, a slight internal pressure build-up was noticed due to a quick pressure relief burst that occurred. However, this appeared to be still very much within the safety margins of the LHTES unit, primarily as no leakage or bursting from the weak points (such as the thermal sensor insertion points) happened at all. Therefore, the pressure resistance and mechanical strength of this analyzed LHTES meant for atmospheric pressure operation seemed to suffice for both RT57HC and RT60HC thermal cycling in the 35-85 °C range. Indeed, the internal pressure resistance and mechanical strength of these LHTES systems are more a design constraint than a material property, but it appears that an LHTES unit designed for maximum 1.5 -2.0 bar,g should suffice for this type systems intended for otherwise atmospheric pressure systems.

7.3. Concluding Remarks - Bench-Scale PCM Testing

As a whole, both RT57HC and RT60HC show very satisfactory properties as PCMs in the bench-scale long-term cycling tests conducted respectively for 25+ (i.e., 27) and 50+ (i.e., 53) cycles. They exhibited no discernible supercooling and only minimal hysteresis. Their thermal energy storage capacities also remained quite consistent throughout these cycles. Whereas, they also exhibited consistent transparent colorless appearance that remained unchanged after the corrosion tests (for both RT57HC and RT60HC) and also after 27 LHTES bulk cycling for RT57HC[7]. These results as a whole imply that both these PCMs present robust cycling stability and no noticeable degradation or ageing for a considerable number of cycles (at least 27 for RT57HC and at least 53 for RT60HC).

The impacts on volume expansion was minimized by filling the PCMs to the LHTES when both are maintained at the highest intended operating temperature. Volume contraction in freezing did not indicate any negative impacts whatsoever. While slight overpressure was felt in the LHTES at heating cycles, it was also found to be within the safety margins of this LHTES meant for atmospheric pressure operations. These imply that these two PCMs do not have any significant vapor pressure and volume expansion impacts and hence do not compromise the mechanical integrity of the LHTES over the analyzed temperatures.

Overall, as both RT57HC and RT60HC showed no perceptible trends of significant variations of the analyzed properties particularly within the bench-scale LHTES long-term cycling tests, it is reasonable to assume that they could be promising as PCMs for long-term application.

[7] RT60HC will be marinated in the same bench-scale set-up for further testing and hence no sampling possible yet

8. Conclusions

Within the work of this deliverable 2.2, the following are achieved, fulfilling the plans and commitments of it quite successfully to a great extent, such as:

- The given requirements were fulfilled during the pre-selection of PCMs, which are biobased and have: high storage capacity, a suitable temperature range, non-corrosive behavior towards the HEX and storage material, high cycle stability and no phase separation
- RT8HC is already a well tested PCM in cold chain logistics and HVAC and has very good themophysical properties as shown in the chapters before. It has a wider temperature range with a sharp solidification peak at 8°C. RT8HC is an organic PCM, biobased and non-corrosive against stainless steel (storage material) and aluminum (heat exchanger).
- Currently ongoing are the storage testing with a polymer heat exchanger of SP12sk and SP45 as inorganic PCMs for solution II with a very good heat storage capacity and sharp temperature peaks. SP45p2 has sharp peaks for melting and solidification and a high storage capacity as shown in Figure 13.
- Long-term bench-scale LHTES testing of the intermediate short-listed PCMs particularly aimed for for HYSTORE solutions I and II: RT57HC and RT60HC both show promise as robust PCMs.
- Specifically, for 25+ (i.e., 27) and 50+ (i.e., 53) cycles, RT57HC and RT60HC respectively exhibited no discernible supercooling and only minimal hysteresis.
- The TES capacities of RT57HC and RT60HC also remained quite consistent throughout these cycles. Their initial transparent colorless appearance also consistently remained unchanged also after the corrosion tests and also after 27 LHTES bulk cycling for RT57HC (with RT60HC further analysis ongoing). Thus, as a whole, it is apparent that RT57HC and RT60HC also have no/negligible ageing (and hence are quite likely chemically stable), for the analyzed amount of cycles.
- The impacts on volume expansion was minimized by filling the PCMs to the LHTES when both are maintained at the highest intended operating temperature. Volume contraction in freezing did not indicate any negative impacts whatsoever. While slight overpressure was felt in the LHTES at heating cycles, it was also found to be within the safety margins of this LHTES meant for atmospheric pressure operations. These imply that these two PCMs do not have any significant vapor pressure and volume expansion impacts and hence do not compromise the mechanical integrity of the LHTES over the analyzed temperatures.
- Based on certain preliminary aspects observed during high-temperature corrosion testing against SS304 and SS316L, RT60HC here shows more promise than RT57HC.
- Overall, as both RT57HC and RT60HC showed no perceptible trends of significant variations of the analyzed properties particularly within the bench-scale LHTES long-term cycling tests, it is reasonable to assume that they could be promising as PCMs for long-term application, with no/minimal ageing.

Some additional reflections per the analyses done and results obtained are:

- The enthalpy characteristics of these PCMs, primarily measured by a calorimetric method, while is adequate to indicate their TES capacities especially during phase change, more accurate complements on specific heat investigations could improve the accuracy of the TES capacity estimations
- LHTES real-scale design implications were identified from the 'artifacts' observed during the bench-scale LHTES cycling. If there's a thermal inhomogeneity in the system with the upper part of the storage unit having a lower temperature than the lower part during melting, at a fast-enough heating rate, displacement of some solid bulk of PCM could happen to the already fully-molten lower points in the TES units. This can most likely affect the overall temperature profile of the LHTES system, indicating an apparent delay that may even appear as a secondary phase change. To avoid this, better temperature distribution and slower heating rates would be helpful.

References

[1] REN21, "Renewables 2019 Global Status Report," REN21 Secretariat, Paris, 2019.

[2] A. Laube, “wärme- und anwendungstechnische Prüfungen Andreas Laube,” [Online]. Available: http://wunda.tech/3-Schicht-Kalorimeter/. [Accessed 04 12 2023].

[3] “Leibniz-Informationszentrum Technik und Naturwissenschaften Universitätsbibliothek,” 2021. [Online]. Available: https://www.tib.eu/de/suchen/id/TIBKAT:1832398765/KOKAP-Kosteneffiziente-Kapselmaterialien-f%C3%BCr-Phasenwechselmaterialien?cHash=174a411d4c3a0697693fc1ab0e1ceaee. [Accessed 29 12 2023].

[4] ASTM International, “NACE TM0169/G31 − 12a: Standard Guide for Laboratory Immersion Corrosion Testing of Metals,” ASTM International, 2017.

[5] ASTM International, “G1 − 03 (Reapproved 2017)- Standard Practice for Preparing, Cleaning, and Evaluating Corrosion Test Specimens,” ASTM International, , West Conshohocken, 2017.

[6] Unilever, “Cif Cream Cleaner Lemon,” Unilever, 2023. [Online]. Available: https://www.cifclean.co.uk/products/catalog/cif-cream-cleaner-lemon-500ml.html. [Accessed 12 December 2023].

[7] VWR International, “Specific gravity cups, calibrated,” 2023 FORTUNE Media IP Limited, 21 11 2023. [Online]. Available: https://se.vwr.com/store/product/12241206/specific-gravity-cups-calibrated. [Accessed 21 11 2023].

[8] Valves Instruments Plus Ltd, “Thermal Expansion,” Valves Instruments Plus Ltd, 2023. [Online]. Available: https://www.vip-ltd.co.uk/Expansion/Thermal_Expansion.pdf. [Accessed 21 11 2023].

[9] S. Laestander, J. Melander, K. N. Bromander and G. Sjöberg, “Thermal Energy Storage Testing - An applied energy project,” KTH Royal Institute of Technology, Stockholm, 2015.

[10] J. Chiu, “Laboratory Handout Latent Heat Thermal Energy Storage Performance Analysis (MJ2386 Energy Storage Technologies),” KTH Royal Institute of Technology, Heat and Power Technology, Stockholm, 2022.

[11] FUCHS LUBRICANTS SWEDEN AB, “RENOLIN THERM 300 X,” FUCHS LUBRICANTS SWEDEN AB, 2023. [Online]. Available: https://fuchs.azureedge.net/fileadmin/se/product-data/renolin-therm-300-x%3Bpds%3Bse-en%3B121504.pdf. [Accessed 13 December 2023].

[12] M. Maurel, “Performance Testing of a Mobile Thermal Energy Storage System,” KTH Royal Institute of Technology, Stockholm, 2017.

[13] SciMed Ltd., “What is Flash Point Testing?,” SciMed Ltd., 2023. [Online]. Available: https://www.scimed.co.uk/education/what-is-flash-point-

testing/#:~:text=Open%20Cup%20Flash%20Point%20Measurement&text=Once%20the%20sample%20material%20is,Cleveland%20open%20cup%20(COC).. [Accessed 13 12 2023].

[14] J. N. Chiu and V. Martin, "Submerged finned heat exchanger latent heat storage design and its experimental verification," *Applied Energy,* vol. 93, pp. 507-516, 2012.

[15] SubsTech, "Stainless steel AISI 304," Substances & Technologies, 13 12 2023. [Online]. Available: https://www.substech.com/dokuwiki/doku.php?id=stainless_steel_aisi_304. [Accessed 13 12 2023].

Appendix A- Material Safety Data Sheets (MSDSs)

The available MSDSs of the final short-listed PCMs RT8HC, RT57HC, RT60Hc and SP31 can be downloaded using the links below.

- MSDS of RT8HC
- MSDS of RT57HC
- MSDS of RT60HC
- MSDS of SP31

Appendix B- Python-based LHTES property calculations

B.1 Dirac function parameter b calculation Python code:

trouverb.py

B.2 RT57HC LHTES property calculation Python code

datacalcRT57HC 2.py

B.3 RT60HC property calculation Python code

datacalcRT60HC (3).py

B.2 Dirac Function parameter *b* calculation procedure:

We need to resolve the following equation :

$$\int_{T_1}^{T_2} \frac{1}{b\cdot\sqrt{\pi}} \cdot e^{-\left(\frac{T-T_{pc}}{b}\right)^2} dT = 0,99$$

We can see that this integral is similar to the Error function :

$$\operatorname{erf} z = \frac{2}{\sqrt{\pi}} \int_0^z e^{-t^2}\, \mathrm{d}t.$$

but we don't have " T^2 " but " $\left(\frac{T-T_{pc}}{b}\right)^2$ "

So we make a substitution of variable :

$$u^2 = \frac{(T-T_{pc})}{b^2}$$

We need to determine the «du» by making the derivative of the equation above.

$$2 \cdot u \cdot du = \frac{2\cdot T - 2\cdot T_{pc}}{b^2} dT$$

$$dT = \frac{b^2 \cdot u \cdot du}{T - T_{pc}}$$

In order to express « dT » with only «u» and «du» we express « T » as a function of «u» .

$$T = b \cdot u + T_{pc}$$

$$dT = b \cdot du$$

Now we can make the substitution in the integral. We have this :

$$\int_{\frac{T_1 - T_{pc}}{b}}^{\frac{T_2 - T_{pc}}{b}} \frac{1}{\sqrt{\pi}} \cdot e^{-u^2} du = 0,99$$

It's almost the expression of the Error function but we need to multiply the equation by 2 and to use the linearity of the integral.

$$2 \cdot \int_{\frac{T_1 - T_{pc}}{b}}^{\frac{T_2 - T_{pc}}{b}} \frac{1}{\sqrt{\pi}} \cdot e^{-u^2} du = 1,98$$

$$\int_0^{\frac{T_2 - T_{pc}}{b}} \frac{2}{\sqrt{\pi}} \cdot e^{-u^2} du - \int_0^{\frac{T_1 - T_{pc}}{b}} \frac{2}{\sqrt{\pi}} \cdot e^{-u^2} du = 1,98$$

Now we have the subtraction of two error functions.

$$erf(\frac{T_2 - T_{pc}}{b}) - erf(\frac{T_1 - T_{pc}}{b}) = 1,98$$

We can't resolve this equation analytically. So we will use the dichotomy method with python.

```python
import math
def erfb(x):
    T1=57
    T2=59
    Tpc=58
    return math.erf((T2-Tpc)/x)-math.erf((T1-Tpc)/x)-1.98
def dichotomie(erfb,a,b,eps):
    if erfb(a)*erfb(b)>0:
        print("False: change your combination of (a,b), erfb(a)*erfb(b) should be <0")
    m=(a+b)/2
    while abs(a-b)>eps:
        if erfb(m)==0.:
            return m
        elif erfb(a)*erfb(m)>0:
            a=m
        else:
            b=m
        m=(a+b)/2
    return m

```

Change the values of T1, T2 and Tpc that you have determined before.
Run the program.
In the console write this :

```
In [2]: dichotomie(erfb,0.01,10,0.000001)
```

And you will have the «b» :

```
Out[2]: 0.5490323689579963
```

OUR TEAM

See you online!

"Funded by the European Union. Views and opinions expressed are however those of the author(s) only and do not necessarily reflect those of the European Union or European Climate, Infrastructure and Environment Executive Agency (CINEA). Neither the European Union nor the granting authority can be held responsible for them."